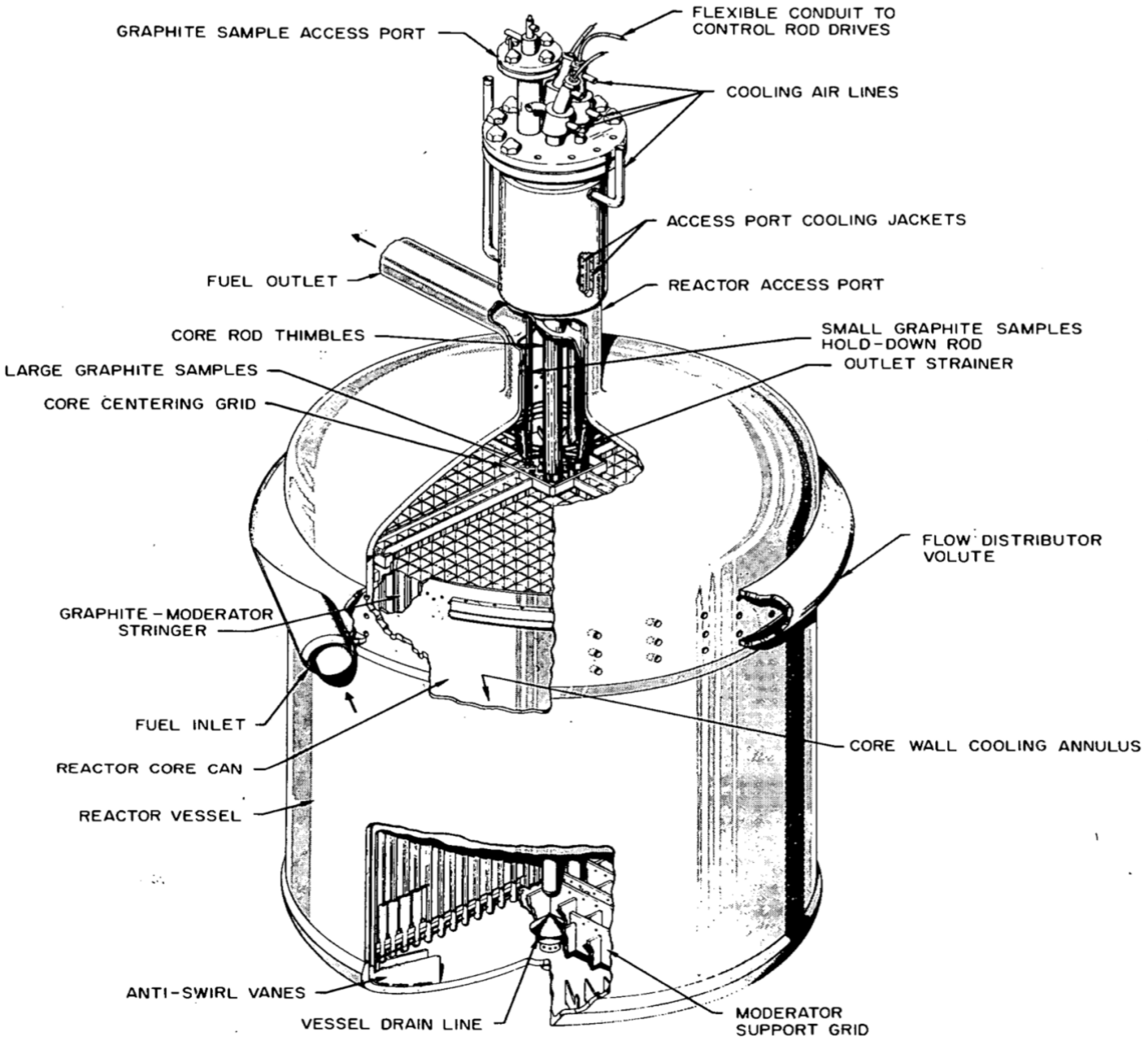

Molten Salt Reactor Experiment Benchmark Evaluation (Project 16-10240)

Massimiliano Fratoni[1], Dan Shen[1]
Germina Ilas[2], Jeffrey Powers[2]

[1]University of California, Berkeley
[2]Oak Ridge National Laboratory

NUCLEAR ENGINEERING
UNIVERSITY OF CALIFORNIA
BERKELEY

Abstract

As one of the six advanced reactor concepts selected by the 2002 Generation IV roadmap as a technology meriting future research, Molten Salt Reactors (MSRs) attracted broad attention and multiple private and public entities are working towards its commercialization. Facing stringent regulatory requirements, validations of computational codes used to calculate and prove the safety characteristics of MSRs play a key role.

This project developed the world-first, MSR-related reactor physics benchmark based on a series of zero-power experiments conducted at the Molten Salt Reactor Experiment (MSRE). The benchmark was succeffully reviewed by the International Reactor Physics Experiment Evaluation Project (IRPhEP) committee and is available in the IRPhEP handbook starting form the 2019 edition.

To benchmark experimental data from the MSRE, a three-dimensional high-fidelity model was developed using the Monte Carlo neutron transport code Serpent 2 and ad-hoc methods have been implemented to account for the unique feature of fuel salt motion. The calculated effective multiplication factor, k_{eff}, for the first criticality experiment, when ^{235}U was progressively added to the fuel salt in order to achieve criticality with stationary salt and isothermal conditions, was 1.02132 (± 3 pcm). The total uncertainty for experimental k_{eff} was estimated to be 420 pcm. The calculated k_{eff} is 2.154% larger than the experimental and benchmark model value, which is approximately five times the benchmark model uncertainty. It is to be noted that, for systems containing large volume of graphite (or other carbonaceous materials), Monte Carlo codes tend to overestimate the k_{eff} of the benchmark model by 1% to 2%. The bias is possibly due to uncertainties in the impurity content of the graphite blocks, uncertainty in the neutron capture cross section of carbon or uncertainty in the properties of nuclear-grade graphite.

The calculated reactivity coefficient of ^{235}U concentration (0.2228 ± 0.0014, represented as the change of reactivity over the relative change of ^{235}U mass in loop) matches well with the experimental value (0.223 ± 0.006), strengthening the confidence on the accurate representation of the fuel salt composition in the MSRE benchmark. Additional reactivity effect calculations, including the control rod bank worth, reactivity effects of fuel circulation and isothermal and fuel temperature coefficients show good agreement with the experimental values (within 1σ) as well.

Contents

Introduction

The fluid-fueled Molten Salt Reactor (MSR) is one of the six advanced concepts selected by the 2002 Generation IV roadmap as a technology meriting future research and development [1]. Since then, several international efforts have carried extensive research and development of MSRs worldwide. In the United States, multiple private ventures, small and large, proponent of various MSR concepts have emerged. The other five Generation IV concepts have all had test reactors constructed, which have provided data to validate simulation codes, and a MSR was also built and operated, providing data that could be used to validate modern simulation models. The Molten Salt Reactor Experiment (MSRE) at the Oak Ridge National Laboratory (ORNL) went critical in 1965 and was operated until 1969 [2]. It was built to demonstrate key features of the molten salt fluid fuel reactors and to prove the practicality of the MSR technology. The experimental program included a variety of criticality and reactivity measurements at zero- and full-power operation for molten-salt fuels using ^{235}U or ^{233}U as fissile material [3, 4]. The wide range of experimental data and documentation available from the MSRE program constitutes a unique and extensive collection of experimental data for this class of advanced reactor concepts.

The International Reactor Physics Benchmark Experiment Evaluation Project (IRPhEP) handbook collects reactor physics experimental data from nuclear facilities worldwide and evaluates those data to develop qualified benchmark data sets for validation of computational methods and techniques [5]. The handbook is prepared by a working party comprised of international reactor physics experts and contains evaluated reactor physics benchmark specifications. The purpose of such specifications is to offer a validation platform for reactor physics computational models, techniques, and data. The 2015 edition included evaluations of data from 143 experimental series performed at 50 nuclear facilities, with 139 evaluations published as approved benchmarks. That edition did not contain any MSR evaluation. Therefore, the University of California, Berkeley (UCB) and ORNL have proposed to develop a set of high-quality MSR reactor physics benchmarks for inclusion in the IRPhEP handbook, using the data archive on the MSRE. In particular, it was proposed to develop an initial IRPhEP benchmark set for the MSRE comprising of the start-up zero power experiments conducted with ^{235}U molten salt fuel. A program of zero-power nuclear experiments was conducted on the MSRE in June 1965 [3]. These experiments were designed to measure basic nuclear characteristics of the MSRE when fueled with ^{235}U and provide a baseline for evaluation of system performance. An initial criticality experiment measured the minimum amount of ^{235}U needed in the LiF-BeF_2-ZrF_4-UF_4 (65.0/29.2/5.0/0.8 mole%) salt mixture in order to achieve criticality under the following conditions: core uniform temperature, stationary fuel salt, and fully withdrawn control rods. More experiments were then conducted at zero-power conditions for gathering information on control rod worth and effects on reactivity of various experimental parameters:

1. Measurements of the differential worth of one control rod were made as a function of position with stationary and circulating salt;

2. The integral worth of various control rod configurations was determined through rod drop experiments;

3. ^{235}U concentration was varied together with control rod positions in order to achieve multiple critical configurations and collect data on ^{235}U concentration reactivity coefficient and control-rod shadowing effects;

4. Stationary and circulating salt conditions were evaluated to establish the effect of fuel salt motion on reactivity;

5. The whole core isothermal temperature reactivity coefficient was measured changing the core temperature at various ^{235}U concentration levels;

6. A pressure reactivity coefficient was measured changing the system overpressure.

The aim of this project was to develop reactor physics benchmarks comprising of all the experiments listed above, including the initial criticality experiment. Such benchmarks were to be developed according to well-established standards and to be included in the IRPhEP handbook. In addition, the following goals were set:

1. Setup a database containing MSRE documentation;

2. Develop computational models for the MSRE;

3. Assess uncertainties both on the experimental data and results, and on the computational results.

The first MSRE benchmark, based on the initial zero-power criticality experiment, was successfully developed and appears in the 2019 edition of IRPhEP handbook [5]. A second revised benchmark including the remaining experiments described above is under review by the IRPhEP committee and is expected to appear in 2020 edition of the handbook.

This report documents in details the efforts carried at UCB and ORNL from October 2016 to December 2019. The report is organized as follows. Section 2 introduces the models and methodologies for benchmarking of the MSRE. After reconstructing the MSRE along with resolving inconsistency among different documentations, a fully-detailed MSRE model was created and the series of MSRE zero-power physics experiment were evaluated step by step. Novel methodologies were developed to model various reactivity effect experiments required in the benchmark. Section 3 summarizes the code-to-experiment validations between Serpent 2, combined with novel methodologies developed to account for unique characteristics in the MSRE benchmark model, and MSRE first zero-power experiments including the criticality experiment and control rod calibration experiments measuring the control rod worth, rod-drop effect, rod-shadowing effect, ^{235}U concentration coefficient of reactivity, effect of fuel salt circulation on reactivity and isothermal temperature coefficients at various ^{235}U concentration levels. Section 5 summarizes the main conclusions and identifies future work.

The Molten Salt Reactor Experiment

2.1 MSRE design features

The MSRE fuel-salt-circulating system is the reactor primary system which consists of the reactor vessel, the fuel circulating pump, the fuel heat exchanger, and the interconnecting piping, as illustrated in Figure 2.1 and Figure 2.2. The major components of this system are contained within the reactor cell, which is a cylindrical carbon steel vessel (7.32 m in diameter and 10.06 m in height), with a hemispherical bottom and a flat top. These components in the reactor cell are laid out in order to be removed by the use of long-handled tools from above [2]. During operation of the reactor, the fuel salt was circulated through the primary system at a rate of 4.54 m^3/min. Table 2.1 provides the volume of each component of the fuel loop and the time that fuel salts requires to flow through each section. Dry, deoxygenated helium gas at 5 psig blankets the fuel salt at the fuel pump bowl and also sweeps the highly radioactive xenon and krypton towards the off-gas disposal system. All metal components were electrically heated to keep the fuel salt molten in zero-power condition. Materials used in the MSRE are summarized in Table 2.2 and the composition of INOR-8 is shown in Table 2.3.

The characteristics of the MSRE are illustrated as follows:

- The homogeneous liquid fuel salt allows online refueling, processing, and fission product removal, avoiding the high cost of fuel fabrication and the need to shut down the reactors for refueling. In addition, lower core excess reactivity can be maintained;
- Fissile materials and most fission products form stable fluorides in the fuel salt, decreasing the risk of severe radioactive release to the environment in an accident. The only exception is the noble metal group which does not form stable fluorides but was found to be plated out on graphite and alloy surfaces exposed to the salt or go into the cover gas above the fuel salt as a smoke or aerosol of sub-micron particles [2]. The high radiation level in the primary loop makes remote maintenance and interior shielding necessary. In the MSRE, there is a thermal shield with a thickness of 40.64 cm surrounding the reactor vessel. It contains 125 tons of steel balls and circulating water to absorb most of the energy of neutrons and gamma ray escaping the reactor vessel. In addition, the MSRE was under remote maintenance. As shown in Figure 2.1, the reactor primary loop and the drain tank system are shielded and installed in containment vessels while the heavily shielded remote maintenance control room is located above the operating floor [6];
- Fluoride salts have reasonably good heat transfer properties, are not damaged by radiation, do not react violently with air or water, and are inert to some common structural metals;
- The high coolant outlet temperature supports high-efficiency electricity production. In addition, the system operates at low pressure (about 5 psig), reducing the capital cost of the reactor vessel;

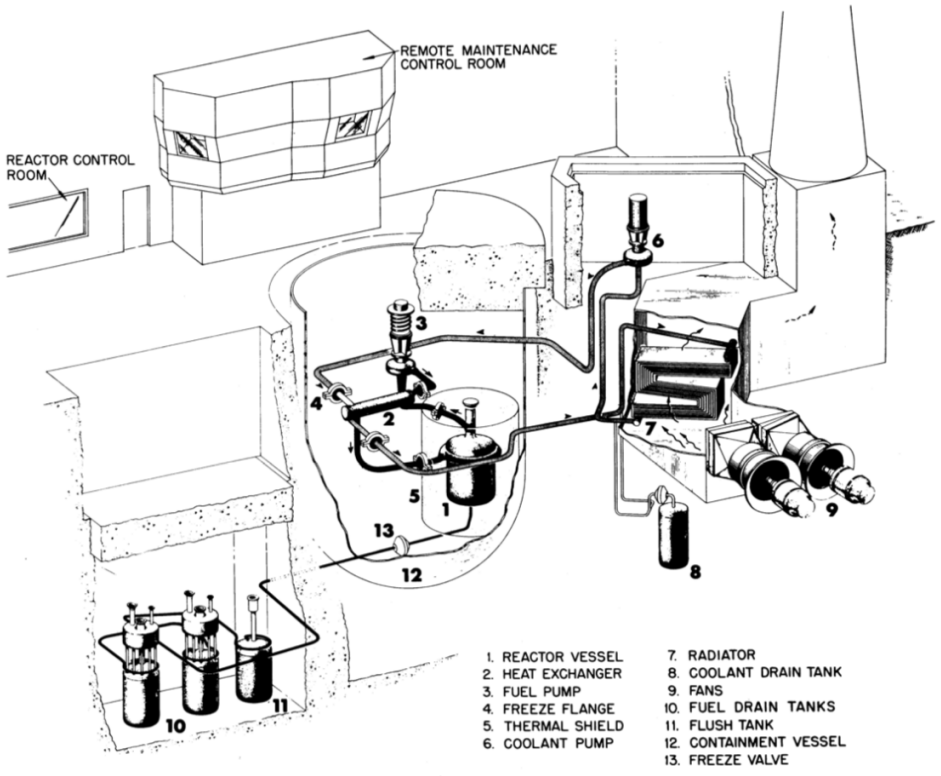

Figure 2.1: MSRE layout [6].

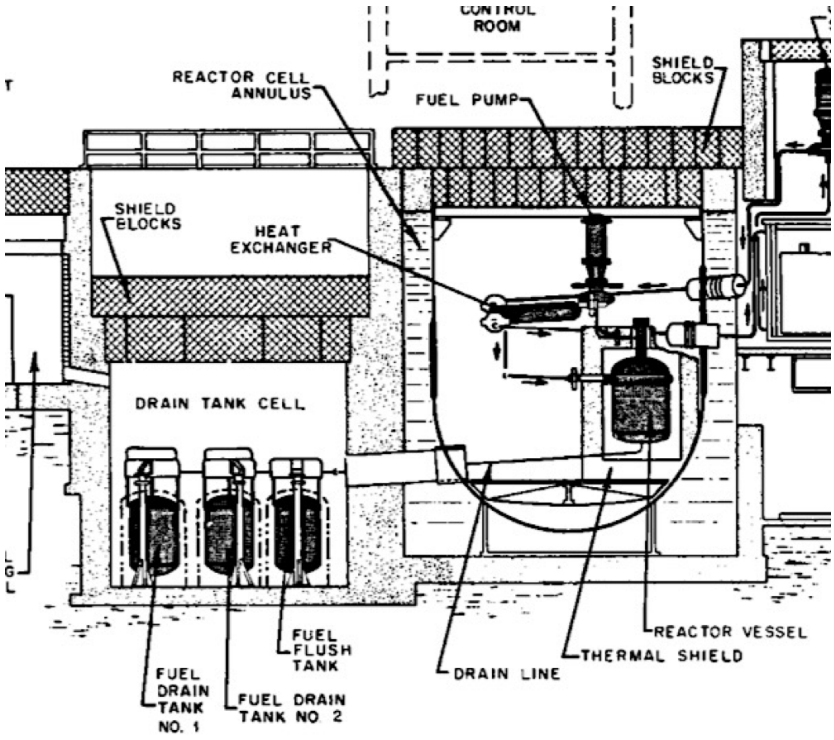

Figure 2.2: Vertical layout of the MSRE reactor cell and drain tank cell [6].

Table 2.1: Salt volume and salt residence times in the components of the fuel loop at 649 °C and 4.54 m^3/min [6].

Component	Volume, m^3	Time, s
Core	0.708	94
Upper head	0.297	39
Reactor vessel to pump	0.059	08
Pump bowl main stream	0.025	03
Pump bowl outside main stream	0.091	–
Pump to heat exchanger	0.023	03
Heat exchanger	0.173	23
Heat exchanger to reactor vessel	0.062	08
Vessel inlet	0.275	36
Lower head	0.283	38
Total in the fuel loop	1.996	252
Total in the fuel loop, drain line and drain tank heel	2.073	–

Table 2.2: Materials used in the MSRE [2].

Component	Material
Fuel Salt	LiF-BeF_2-ZrF_4-UF_4
Coolant salt	LiF-BeF_2
Moderator	Graphite
Salt containers	INOR-8
Cover gas	Helium

Table 2.3: Composition of INOR-8 used in the MSRE [6].

Element	Mass fraction,%
Ni	66 to 71
Mo	15 to 18
Cr	6 to 8
Fe, max	5
C	0.04 to 0.08
Ti + Al, max	0.50
S, max	0.02
Mn, max	1.0
Si, max	1.0
Cu, max	0.35
B, max	0.010
W, max	0.50
P, max	0.015
Co, max	0.20

- The system has good neutron economy. The use of unclad graphite in the core and the rapid removal of gaseous fission products result in good fuel utilization, avoiding control problems of xenon poisoning as a bonus;
- Inherent safety in the MSRE is afforded by the design of freeze valves. Salt was introduced into the primary circulating system or drained from it through the vessel drain line running from the bottom of the reactor vessel (see Figure 2.3). The valve controlling the drain line is a freeze valve which was closed by a frozen plug of salt. When a drain is requested, the temperature of the freeze valve in the drain line will be increased and the frozen salt plug will be thawed in 10 to 15 min. A power failure accident can also result in a drain because the cooling air required to keep the valves frozen is interrupted [2].

The MSRE reactor vessel is compact, with an inner diameter of 147.32 cm and a height of 233.90 cm (as shown in Figure 2.3 and Figure 2.4). The fuel salt enters the flow distributor through the fuel inlet, which is arranged tangentially to the top of the vessel. The flow distributor is half-circular in cross section with an inside radius of 10.16 cm. The fuel is distributed evenly around the circumference of the vessel while passing the flow distributor and then flows turbulently downward in a spiral path through a 2.54 cm wide annulus between the vessel wall and the core can. The salt loses its rotational motion in the 48 straightening vanes in the lower plenum and flows upward through the graphite matrix in the core can. Elimination of the swirl in the bottom head reduces the radial pressure gradient and promotes even flow distribution through the core.

The reactor vessel has two torispherical domes with 147.32 cm inner diameter and 2.54 cm thickness as the upper and lower plenum. The wall thickness of the cylindrical portion of the vessel is 1.429 cm, except for the top 40.64 cm of the vessel, which has a wall thickness of 2.54 cm. The core can, or core container, inside the vessel has an inner diameter of 140.97 cm and was rolled from 0.635 cm thick INOR-8 plate. The core can is supported, and also held down when salt is in the reactor, by a ring at the top which is bolted to 36 lugs welded to the inside wall of the reactor vessel. The can, in turn, supports the graphite in the reactor.

The graphite matrix is an assembly of vertical stringers with a 5.08 cm by 5.08 cm cross section as shown in Figure 2.5. Fissioning occurs when the fuel salt flows through the channels formed by grooves in the 4 sides on the stringers. These channels are 1.016 cm by 3.048 cm with round corners of radius 0.508 cm (see Figure 2.6). The graphite stringers are 170.03 cm long and are mounted in a vertical close-packed array. There are a total of 1140 equivalent full-size passages, counting fractional sizes. The dimensions of the flow channel were chosen to provide a passage that would not be blocked by small pieces of graphite and also to obtain a nearly optimum fuel-to-graphite ratio in the core.

The MSRE graphite has an average density of $1.86\,g/cm^3$, lighter than the salt density which is approximately $2.3275\,g/cm^3$. When not buoyed up by being immersed in the fuel salt, the vertical graphite stringers rest on a lattice of graphite blocks, with a 2.54 cm by 4.1275 cm cross section, that is laid horizontally in two layers at right angles to each other. Holes in the lattice blocks, with a diameter of 2.642 cm, accept the 2.54 cm diameter doweled section at the lower end of each stringer. The upper horizontal surface of the vertical graphite stringers is tapered to ensure no salt remains after on it after a salt drainage as shown in Figure 2.5.

Four graphite stringers were left out to leave space for three control rod thimbles and a surveillance assembly consisting of graphite and INOR-8 sample baskets, which are arranged equidistantly near the center of the core as shown in Figure 2.7. One of the objectives of the MSRE was to investigate the behavior of the uncladded graphite moderator and INOR-8 in the reactor environment. Thus, the reactor was designed for periodic removal of graphite specimens from near the center of the core. The five graphite stringers enclosed by the control rods and sample baskets, labeled 7, 60, 61 in Figure 2.7, are of a special design so that they could be easily removed out of the core for examination. In the surveillance assembly, there are three identical sample baskets

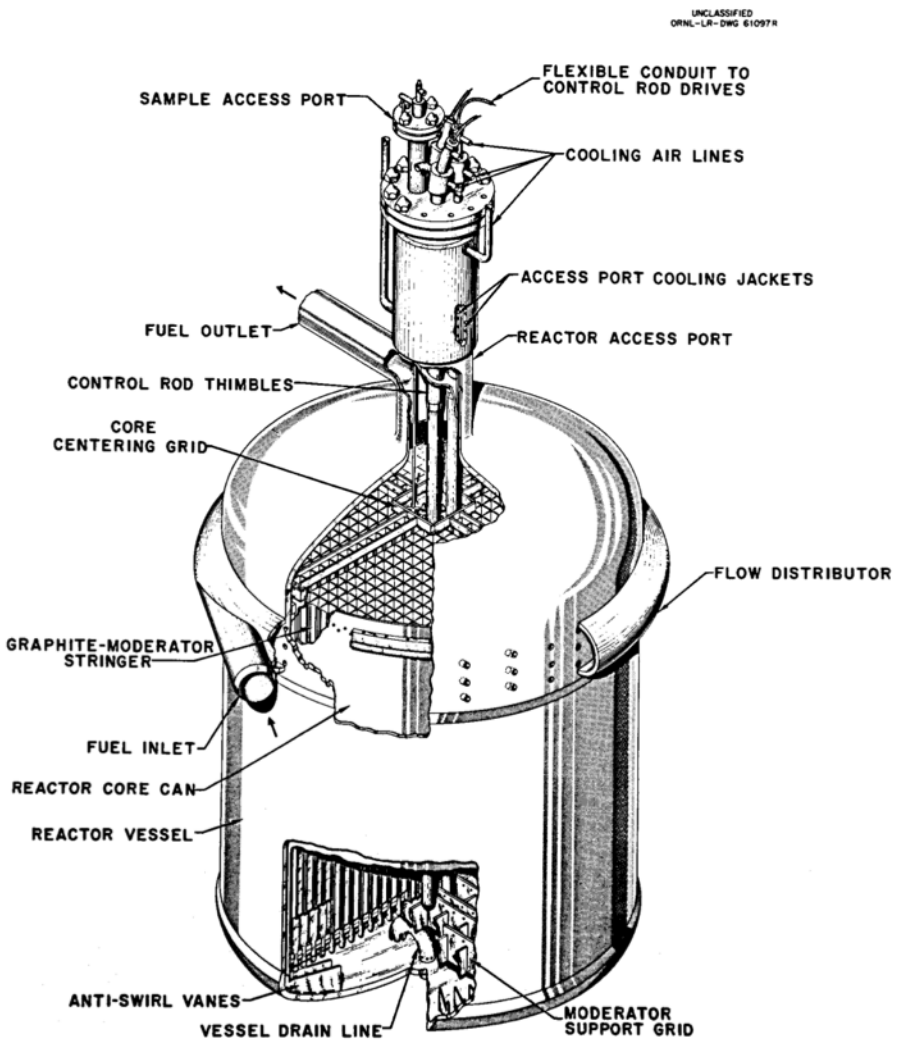

Figure 2.3: Cutaway of the MSRE reactor vessel[6].

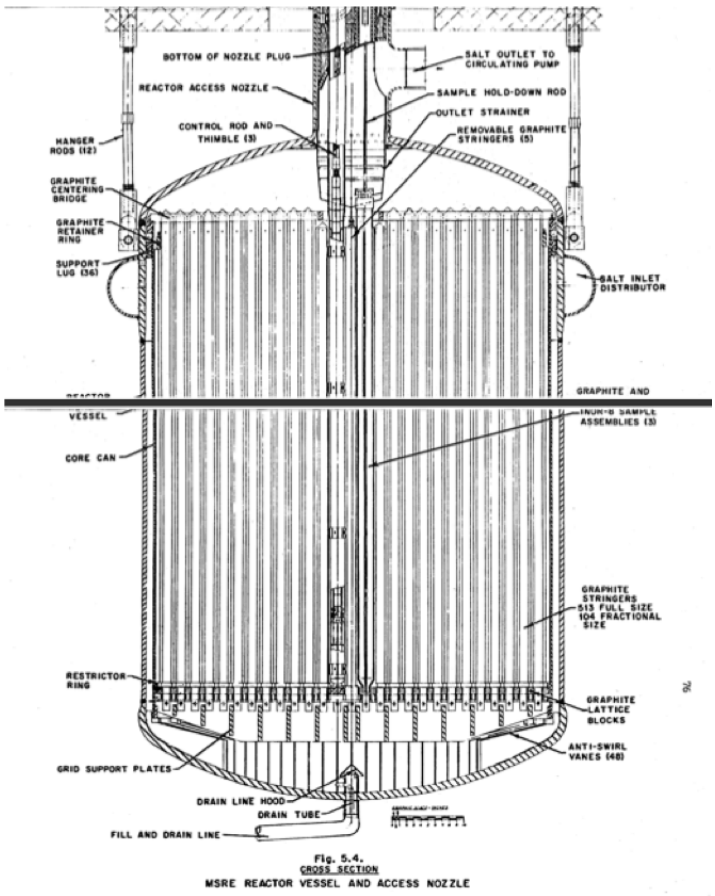

Figure 2.4: Vertical cross section of the MSRE vessel[6].

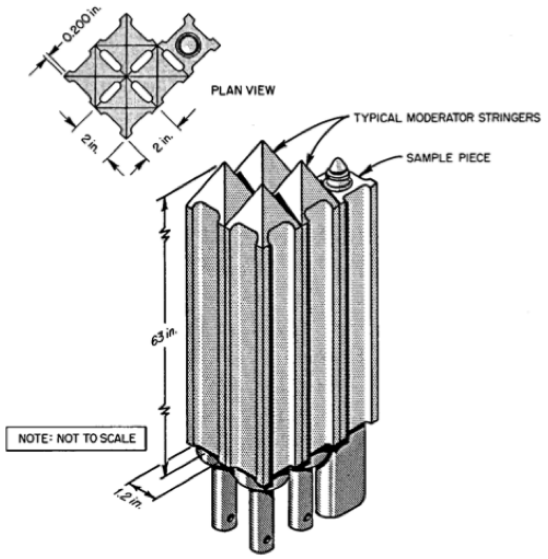

Figure 2.5: Dimensions and arrangement of the graphite stringers[6].

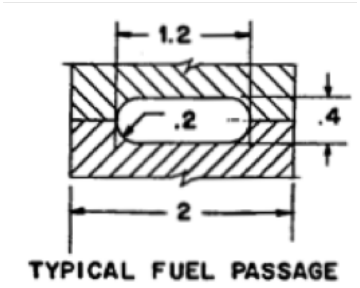

Figure 2.6: Dimensions and arrangement of the fuel channel (the unit of length is inch)[6].

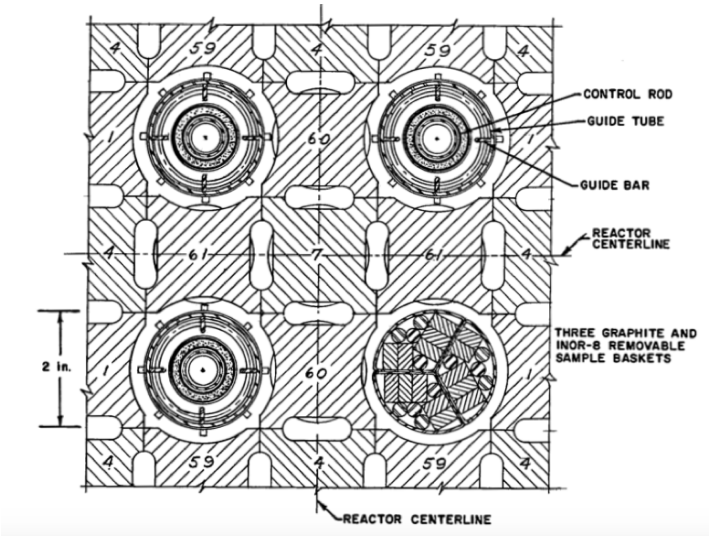

Figure 2.7: Control rod and sample baskets of the MSRE[6].

mounted vertically and each basket is formed of 0.079-cm-thick INOR-8 plate and has 0.238-cm-diameter holes and contains four 0.635-cm diameter and 167.64-cm long samples of INOR-8, and five graphite sample bars 0.635 cm $\times$ 1.1938 cm with a length of 167.64 cm.

The control rod thimbles have a 5.08-cm outer diameter and 0.1651-cm thick wall tubing. The control rods are segmented (see Figure 2.8 and Figure 2.9) to provide the flexibility needed to pass through the bends in the control rod thimbles (see Figure 2.10). The poison material is a mixture of 70 wt % Gd_2O_3 and 30 wt % Al_2O_3. Three ceramic cylinders are canned in an Inconel shell to form one control rod element. Each control rod is made of 38 elements for total length of the poison section of 150.774 cm. The segments are threaded, bead-like, on a 1.905-cm outer diameter by 1.5875-cm inner diameter helically wound, flexible stainless steel. Two 0.3175-cm diameter braided Inconel cables run through this hose to restrain it from stretching when dropped in free fall. This hose passes upward through the thimble to the positioning chain on the control-rod drive mechanism. A position indicator is provided for the lower end of the rod which permits re-calibration of the position-indicating devices related to the upper end of the rod, should there be variations in the length.

The reactor vessel is installed in a thermal shield that supports the vessel and forms the outer wall of the reactor furnace. The shield, consisting of a tank of stainless steel filled with steel balls and circulating water, has an approximate outer diameter of 317.5 cm, an inner diameter of 236.22 cm and a height of 383.54 cm, as shown in Figure 2.11. Besides absorbing energy of

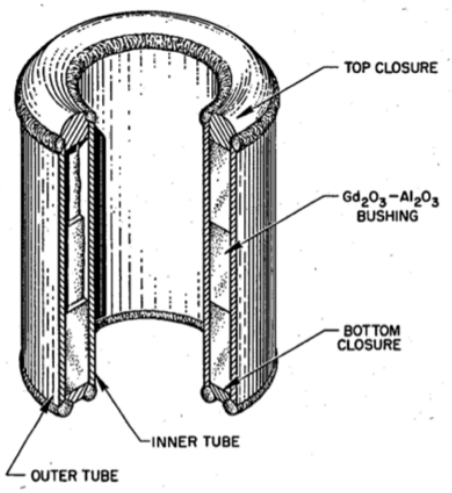

Figure 2.8: Cutaway of an MSRE control element[7].

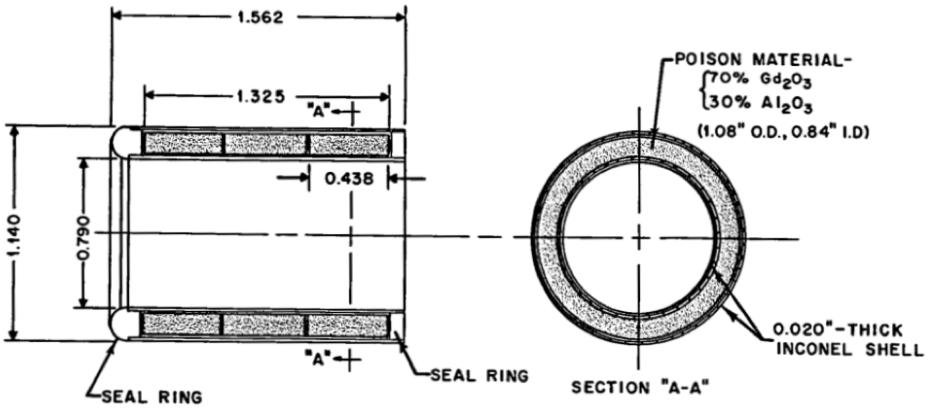

Figure 2.9: Control rod poison element geometry (the unit of length is inch)[6].

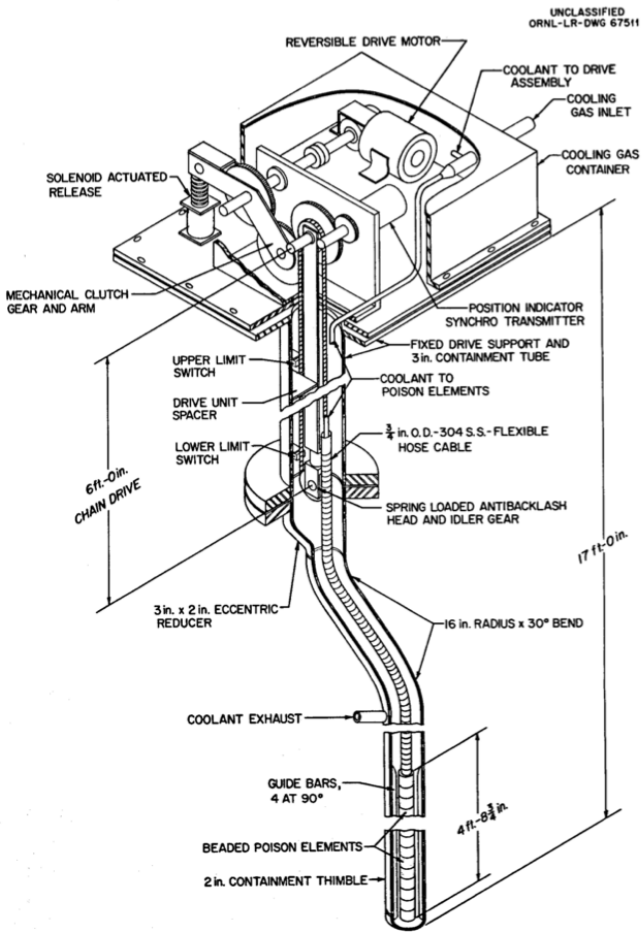

Figure 2.10: Control rod and drive[6].

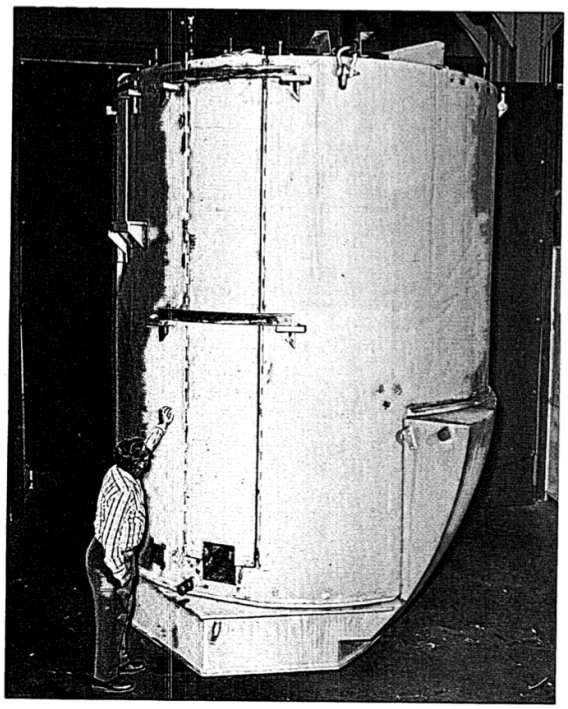

Figure 2.11: Image of the thermal shield [6].

neutrons and gamma ray escaping from the core, the shield also cuts down on neutron activation of components in the reactor cell [2]. The inside of the thermal shield is lined with 15.24 cm of high temperature insulation (vermiculite). And the reactor vessel is supported from the top removable cover of the thermal shield.

2.2 Initial zero-power criticality experiment

ORNL conducted a program of zero-power nuclear experiments on the MSRE in June 1965 to establish the basic nuclear characteristics of the reactor system and to provide a baseline for evaluation of the system performance during operation [3].

This program started from the first criticality experiment that established the initial critical ^{235}U loading under the simplest possible conditions, that is, with core isothermal, fuel salt stationary and control rods withdrawn to their upper limits. The first criticality experiment basically consisted in adding increments of enriched uranium concentrate to the fuel salt, LiF-BeF_2-ZrF_4-UF_4, and observing the progress toward the critical concentration by the increased neutron source multiplication. Successive additions of kilogram quantities of ^{235}U to the salt in the drain tanks, followed each time by a fill of the core and multiplication measurements, occurred until the reactor contained approximately 98 % of the critical mass. The remainder was added in 85-g batches through the sampler-enricher. The sampler-enricher system can lower small capsules into the pump bowl to take samples from or add salt into the main circulating stream. Four neutron counting channels were used: two fission chambers in the instrument shaft, a BF_3 chamber in the instrument shaft, and another BF_3 chamber in the thermal shield as shown in Figure 2.12.

The salt was prepared in three lots: (1) carrier salt (65LiF-30BeF_2-5ZrF_4, salt compositions are expressed in mole percent), containing the beryllium, zirconium and most of the lithium fluorides; (2) depleted uranium eutectic (73LiF-27UF_4), containing 150 kg of depleted uranium; and (3)

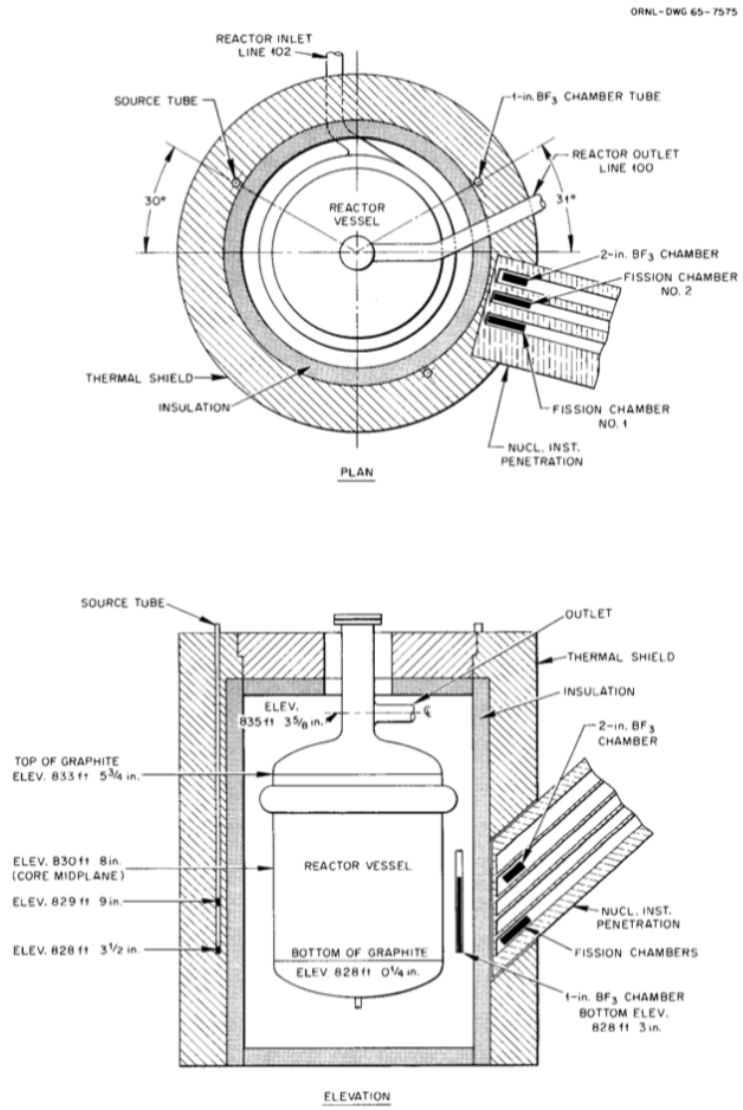

Figure 2.12: Source and instrumentation in initial criticality experiment[3].

.

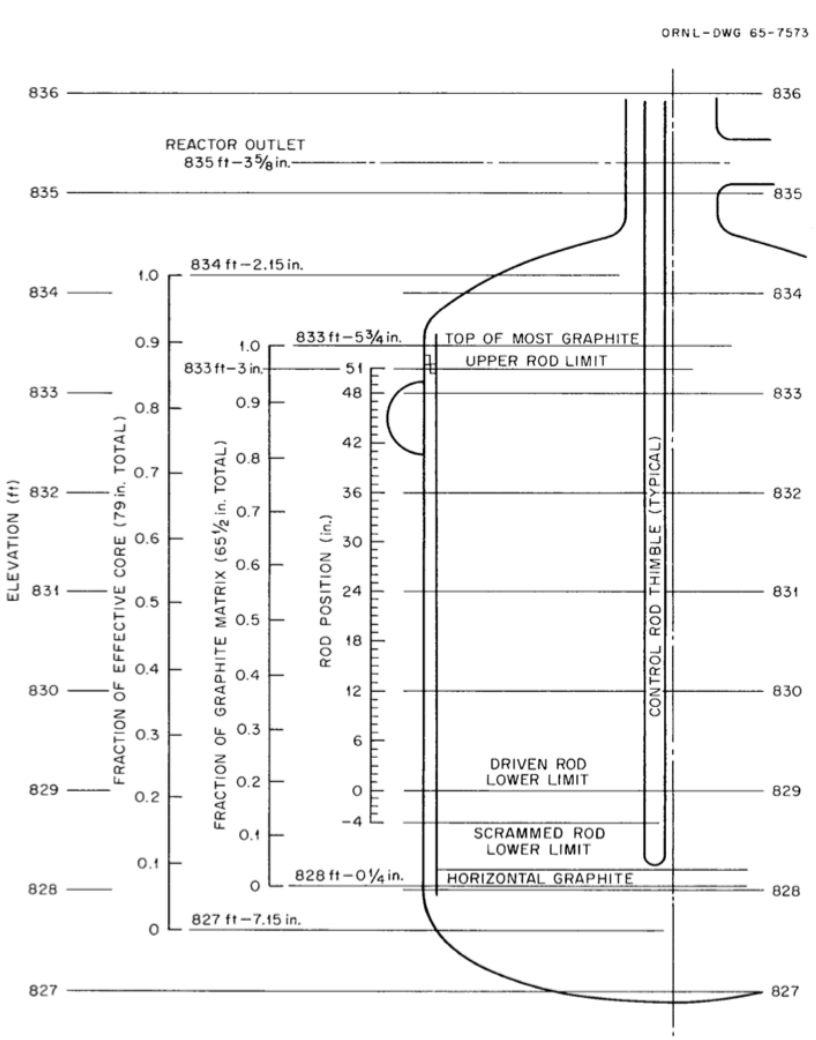

Figure 2.13: Relation of rod position and levels in reactor vessel [3].

highly-enriched eutectic, containing 90 kg of ^{235}U at 93 % ^{235}U enrichment. Thirty-five cans of carrier salt (containing 4558.1 kg of carrier salt) and two cans of depleted uranium eutectic (containing 236.2 kg of LiF-$^{238}UF_4$) were blended as they were charged into a drain tank [8]. This mixture of salt was then circulated for ten days at 649 °C while the sampler-enricher was tested, and 18 samples were analyzed to establish the initial composition. The criticality experiment then consisted in progressively increasing the enriched uranium content to bring the ^{235}U concentration up to the critical point.

On June 1, 1965, at approximately 6:00 pm, the reactor reached the critical point with fuel salt stationary [3]. Criticality was verified by leveling the power at successively higher level with the same rod position. The actual system power was about 10 W. The mass fraction of ^{235}U in the fuel salt was (1.408 ± 0.007) wt % after considering the small amount of dilution of the fuel salt from residues of flush salt left in freeze valves and drain tank heels when the fuel salt was charged. The core temperature at the time of criticality was measured to be 638 °C instead of 649 °C as initially estimated. The fuel salt density was (2.3275 ± 0.0160) g/cm^3. One rod was inserted at 46.6 in. (the relation of rod position in the control rod thimble and elevations is shown in Figure 2.13) while the other two rods were held at 51 in., the upper limit.

2.3 Reactivity effects and reactivity coefficients measurements

Following the initial zero-power criticality experiment conducted on the MSRE in June, a series of control rod calibration experiments measuring reactivity effects were performed by ORNL.

The general method of increasing the uranium concentration in the fuel salt was to add 85 g ^{235}U in a capsule at a time through the sampler-enricher. The insertion of the regulating control rod (rod No. 1, the top right rod in Figure 2.7) always acts to follow and compensate for any net excess reactivity from the additions of uranium or any change of the core configuration. Figure 2.14 depicts the procedure of these control rod calibration experiments. Each curve in Figure 2.14 is a qualitative graphical description of the change in the static reactivity as a function of regulating rod position and various curves represent different ^{235}U loadings, increasing in the direction shown by the arrow. The static reactivity, ρ_s, corresponding to each specific rod position and ^{235}U loading is defined by the following equation:

$$\rho_s = \frac{\nu - \nu_c}{\nu} \tag{2.1}$$

where ν is the actual number of neutrons emitted per fission, and ν_c is the fictitious value for which the reactor with the specified rod position and material composition, and with the fuel stationary, would be just critical. An equivalent expression is:

$$\rho_s = \frac{k_{eff} - 1}{k_{eff}} \tag{2.2}$$

where k_{eff} is the effective multiplication constant of the reactor.

There are two types of kinetic measurements occurred, the stable period measurement for the period-differential control rod worth experiment and the rod-drop experiment:

- A typical measurement of the stable period corresponds to a motion of the control rod from its critical position upward (same as moving to the left along the short segment marked (p) in Figure 2.14). The measured change in reactivity along the vertical axis, ρ_p, is divided by the increment in rod motion, and this differential worth is ascribed to the mean position;
- A typical rod-drop experiment is indicated in Figure 2.14 by the segment marked (d), extending from the initial critical control rod position into the subcritical region. The purpose of this experiment is to measure the negative reactivity inserted by the drop, marked ρ_d.

Figure 2.15 depicts the parameter region of the rod calibration experiments in the MSRE. The solid curve oc lying in the horizontal plane (reactivity = 0) is the only relation directly accessible from experiments[9]. To obtain knowledge of the complete surface S, it is necessary to "reach" into the vertical dimension, either by performing kinetic experiments or by performing theoretical calculations.

According to [9], the static reactivity concept, which often used to describe the off-critical state, can be relate to the reactivity inferred from kinetic measurements if the model used is sufficiently realistic and can give an exact description of the critical state. For the period-differential worth and rod-drop integral-worth experiments in the MSRE, the differences in the static reactivity, defined by Eq. 2.1, and the reactivity inferred from kinetic measurements are operationally insignificant. The use of correction factors, wherever necessary to keep consistency in the uranium concentration, and the design of measurement procedures that avoids instances where important differences between the two kinds of reactivity can occur achieve the goal. Therefore, the static reactivity concept and scale was regarded as a basis for an integrated and unified interpretation of the measured reactivity for the MSRE.

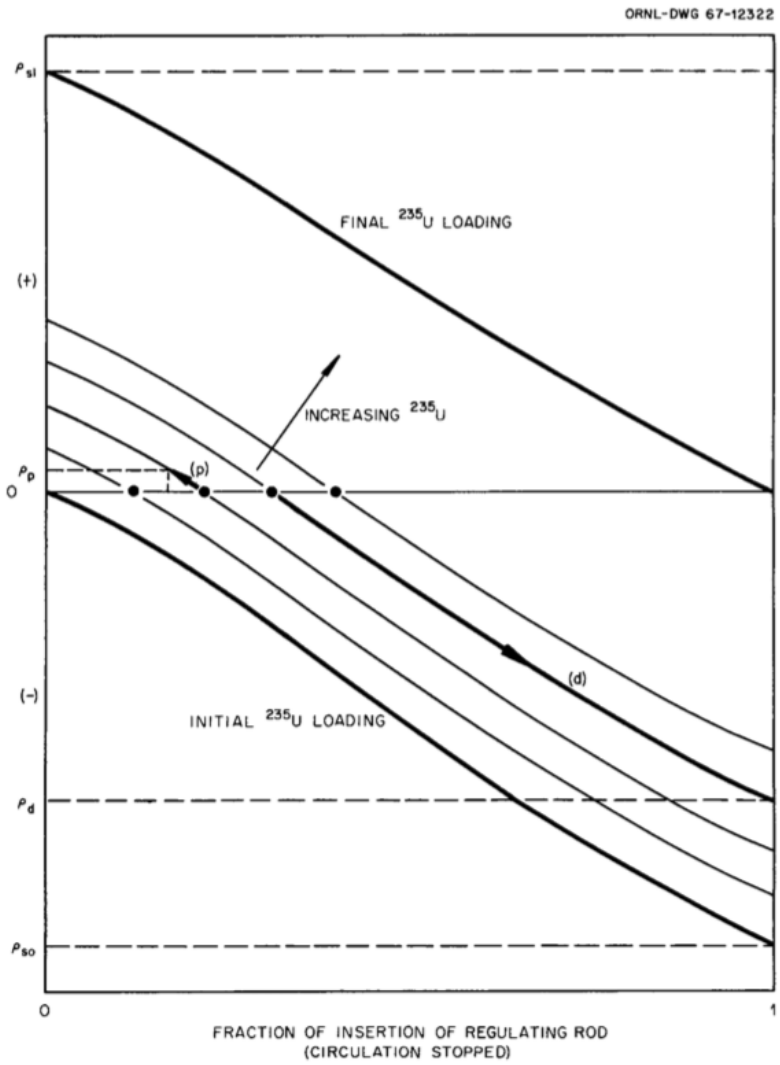

Figure 2.14: Graphical description of control rod calibration experiments[3].

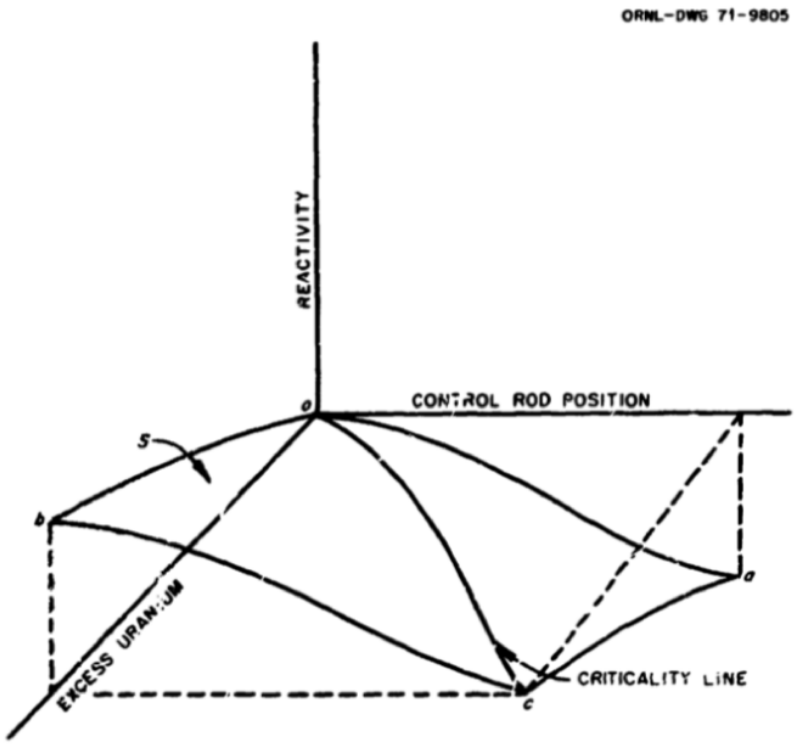

Figure 2.15: Parameter region in zero-power rod-calibration experiments[9].

The detailed descriptions of MSRE control rod calibration experiments can be found in [3] or in the official MSRE benchmark for the IRPhEP handbook. A brief overview is provided here.

First of all, the differential reactivity worth of control rod No. 1 as a function of position was measured, both with the fuel salt stationary and with it circulating. At the same time, the critical control rod configurations as a function of uranium concentration were obtained and the reactivity equivalent of ^{235}U additions can be determined from the previous rod worth measurement. As shown in Figure 2.14 and Figure 2.15, only the reactivity equivalent of the ^{235}U addition was compensated by insertion of control rod. Therefore, calibration of the rod by independent experiments can provide an empirical determination of the reactivity worth of the additional ^{235}U. Following that, the effect of fuel salt circulation on reactivity and control rod shadowing effects were measured. The control rod shadowing effects refer to the change in the critical position of the regulating rod (rod No. 1) as the shim rods (rods No. 2 and No. 3) were inserted into the core. Rod-drop experiments were performed to provide an independent verification of the integral worth of various control rod configurations. Sufficient excess uranium was added during this program to permit calibration of one control rod over its entire length of travel. The final amount of ^{235}U was to be enough to be critical at 649 °C with the fuel stationary and one rod fully inserted.

The isothermal temperature coefficient and fuel temperature coefficient were measured basing on the results of control rod calibration experiments. At three fixed ^{235}U concentrations, the reactor system temperature was varied slowly (about 15 °F/h) by adjusting electric heaters while the critical position of the regulating rod was observed. The change in critical position of the regulating rod was converted to reactivity by use of the rod calibration results. This experiment gave the overall temperature coefficient, that is, the sum of fuel and graphite coefficients.

An attempt was made to separate the fuel (rapid) and graphite (sluggish) temperature coefficients by an experiment in which the fuel was kept in circulation and the coolant loop was stagnant. After heating the stagnant coolant salt about 20 °F hotter than the fuel salt, the coolant pump was started, introducing a hot slug of fuel into the heat exchanger and subsequently into the core. In this test, then, the change in reactivity was due entirely to the change in fuel temperature.

As the essential basis for all the following experiments, the stable period measurements for rod differential worth is further illustrated here.

At certain ^{235}U concentration level, the control rod No. 1 was first adjusted to make the reactor critical at about 10 W and then it was pulled a prescribed distance and held there until the power had increased by about two decades. Two fission chambers driving log-count-rate meters and a two-pen recorder were used to measure the period (generally in the range of 30 sec to 150 sec). For the measurements with the pump off, the standard inhour relation was used to calculate the reactivity increment corresponding to ω, the observed stable inverse period, as below:

$$\rho = \omega\Lambda + \sum_{i=1}^{6} \frac{\beta_i \omega}{\omega + \lambda_i} \tag{2.3}$$

The decay constants, λ_i, and the effective delay fractions, β_i, used in these calculations, are listed in Table 2.4. The neutron generation time, Λ, was 2.6×10^{-4} sec for the initial critical loading, obtained from theoretical analysis [3].

The differential-worth measurements made with the fuel pump off are plotted in Figure 2.16. Theoretical corrections have been applied to these measurements to put them all on the basis of one ^{235}U concentration, arbitrarily chosen as the initial critical concentration that is 65.25 kg ^{235}U in loop. The approximate correction factors which were applied to the rod sensitivity measurements increase linearly with ^{235}U concentration, up to 1.087 for the measurements made near the final concentration that is 71.71 kg ^{235}U in loop. As stated before, it is useful for purposes of consistency to interpret the combined reactivity measurements, over the whole range of rod movement, on the basis of a single mass of ^{235}U. Theoretical calculations of the rod worth by ORNL were used

Table 2.4: Delayed neutron fractions used for reactivity inference in MSRE differential rod worth measurements [3].

Group	Decay constant, s^{-1}	Actual delay fraction $\times 10^4$	Effective delay fraction[a] $\times 10^4$
1	0.0124	2.11	2.23
2	0.0305	14.02	14.57
3	0.1114	12.54	13.07
4	0.3013	25.28	26.28
5	1.140	7.40	7.66
6	3.010	2.70	2.80

[a] With fuel stationary.

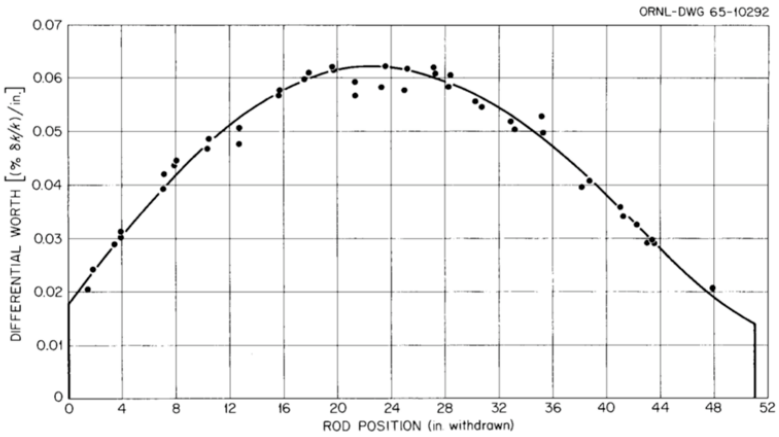

Figure 2.16: Differential worth of control rod No. 1, measured with fuel stationary and normalized to initial critical ^{235}U loading[3].

to determine the effects of the ^{235}U concentration on the rod worth.

Serving as an independent check for the integral worth of various control rod configurations, the rod-drop experiment is further illustrated here.

After 30, 65 and 87 capsules of enriched uranium additions, rod-drop effects were observed, which consists of the intentional scram of a rod, or rod group, from an initially critical configuration and the recording of the decay of the neutron flux as a function of time following the scram. The flux decay trajectory is characterized by a sharp drop immediately following the scram, corresponding closely with the actual fall of the rod. After that, the curve rapidly and continuously evolves into one with a much slower rate of flux decrease, governed by the decay of the initial distribution of delayed neutron precursors (DNPs). The integral neutron count, rather than log n, as a function of time following the rod drop was recorded to serve the requirements of fast response, good counting statistics, and reproducibility. The results of the rod-drop experiments made after additions of 30 and 65 capsules of enriching salt are shown in Figure 2.17 and Figure 2.18.

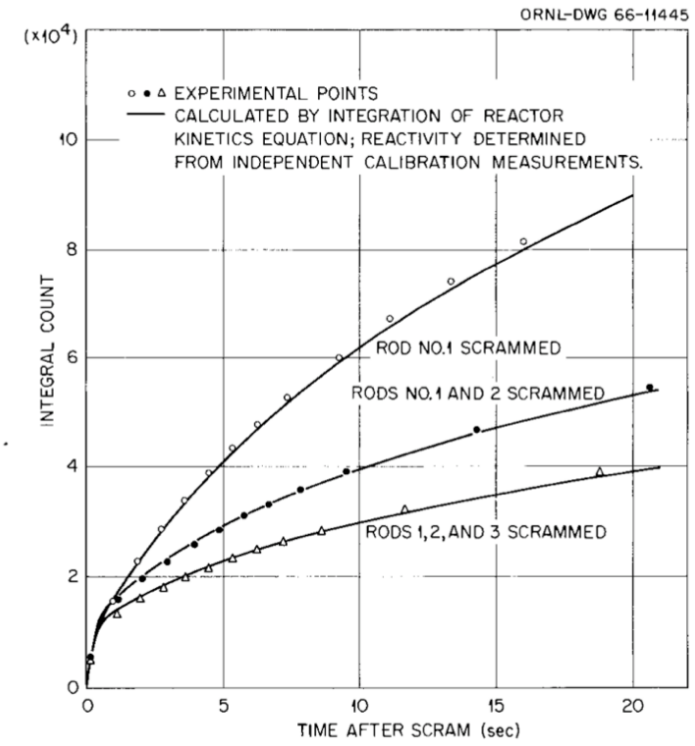

Figure 2.17: Results of rod-drop experiments after 30 capsule additions[3].

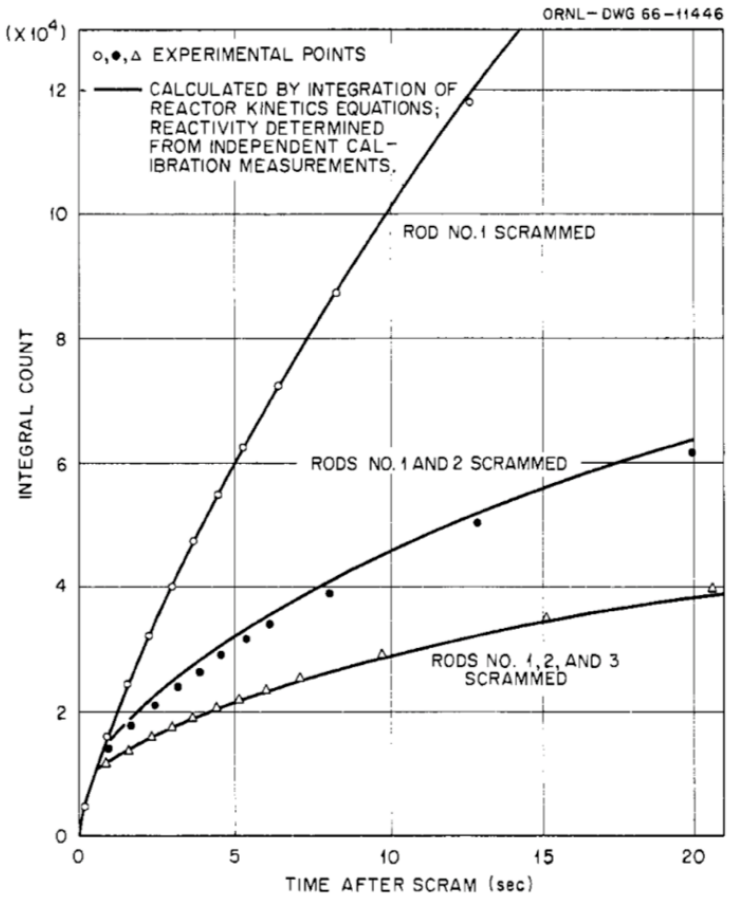

Figure 2.18: Results of rod-drop experiments after 65 capsule additions[3].

Computational models

3.1 Serpent 2 model

A benchmark model of the MSRE first criticality experiment was prepared and analyzed by Serpent 2 with as much detail as feasible. In this benchmark model, the dimensions for the graphite lattice, control rod thimbles, sample baskets, reactor vessel shell, flow distributor and thermal shield are those obtained from design data and/or blueprints while the fuel inlet pipe, fuel outlet pipe, fuel outlet strainer, reactor access port (Figure 2.3), the external loop outside the thermal shield and the base for the thermal shield are neglected. The bias from neglecting these components in the benchmark was evaluated by creating a fully-detailed model (see Figure 3.1) which contains the fuel inlet pipe, fuel outlet pipe, fuel outlet strainer, reactor access port and thermal shield base and the biases on k_{eff} was calculated to be (-22 ± 5) pcm.

There are other simplifications in the MSRE benchmark model which are believed to have no significant effect on k_{eff}. The lower head of the reactor vessel is simplified as a homogeneous mixture of fuel salt and INOR-8 with a volume ratio of 90.8:9.2 according to [10]. The upper head of the reactor vessel is simplified to a pure salt region. The insulation layer and thermal shield are also simplified as homogeneous mixture.

All the dimensions are “hot" dimensions (at 638 °C) in the benchmark model. Since all the dimensions provided in the reference were at room temperature, the thermal expansion of graphite and metal components was performed in the reactor vessel from 20 °C (the room temperature) to 638 °C (the operating temperature) of the experiment. According to [6], the thermal expansion coefficient for graphite lattice is $1.5 \times 10^{-6}\,°\mathrm{F}^{-1}$ and is $7.8 \times 10^{-6}\,°\mathrm{F}^{-1}$ for metal components. To simulate the thermal expansion, the reactor vessel was freely expanded downward from the interface between the outlet pipe and the upper insulation layer, as shown in Figure 2.12. The horizontal graphite lattice was connected with the vessel at its bottom, labeled as $z = 0$ plane in the model, and the vertical graphite stringers were held by the horizontal graphite lattice; therefore, in the benchmark model considering thermal expansion, the horizontal graphite lattice was first moved together with the vessel to a new $z = 0$ plane and then thermally expanded upward from the $z = 0$ plane. Finally, the thermally expanded vertical graphite stringers were put upon the horizontal graphite lattice.

Figure 3.2 and Figure 3.3 provide an overview of the benchmark models, including axial location respect to the bottom of the horizontal graphite lattice and radial dimensions. The arrangement of the graphite stringers is disrupted in the center by three control rods and the sample baskets as shown in Figure 3.4. The control rods and sample baskets are housed in a cylindrical channel of 3.1992 cm radius. The space in between the graphite and the control rod thimbles and basket is filled with salt.

As the most important component in the core geometry, the vertical graphite lattice is formed by vertical graphite stringers whose cross section is a square with side length of 5.083 39 cm; 1.017 70 cm by 3.053 09 cm fuel channels with round corners (radius is 0.508 85 cm) are machined at the center the four sides of the stringers as shown in Figure 3.5. At the boundary of the lattice some stringers are cut and some channels are partially closed, as shown in Figure 3.6, according

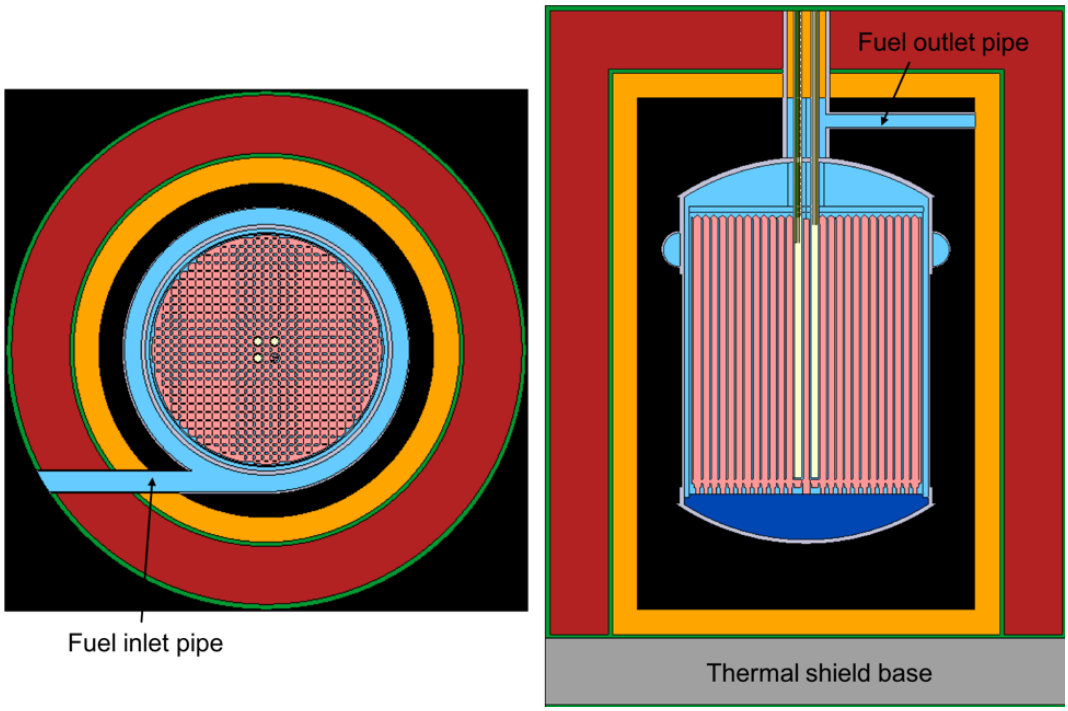

Figure 3.1: Horizontal cross section at $z = 145.396\,\text{cm}$ (left) and vertical cross section of the core offset by $5.083\,39\,\text{cm}$ from the center (right) of the full detailed MSRE model.

Table 3.1: Comparison of "cold" and "hot" dimensions of the MSRE.

Dimension	Cold (20 °C)	Hot (638 °C)
Graphite lattice radius, cm	70.168	70.285
Core can inner radius, cm	70.485	71.097
Core can outer radius, cm	71.120	71.737
Reactor vessel inner radius, cm	73.660	74.299
Reactor vessel outer radius, cm	76.200	76.862
Graphite stringer width, cm	5.075	5.084
Fuel channel width, cm	1.016	1.018
Fuel channel length, cm	3.048	3.053
Graphite stringer height, cm	170.027	170.311
Total height of the vessel, cm	269.771	272.113
Length of the control rod inserted, cm	76.414	77.077

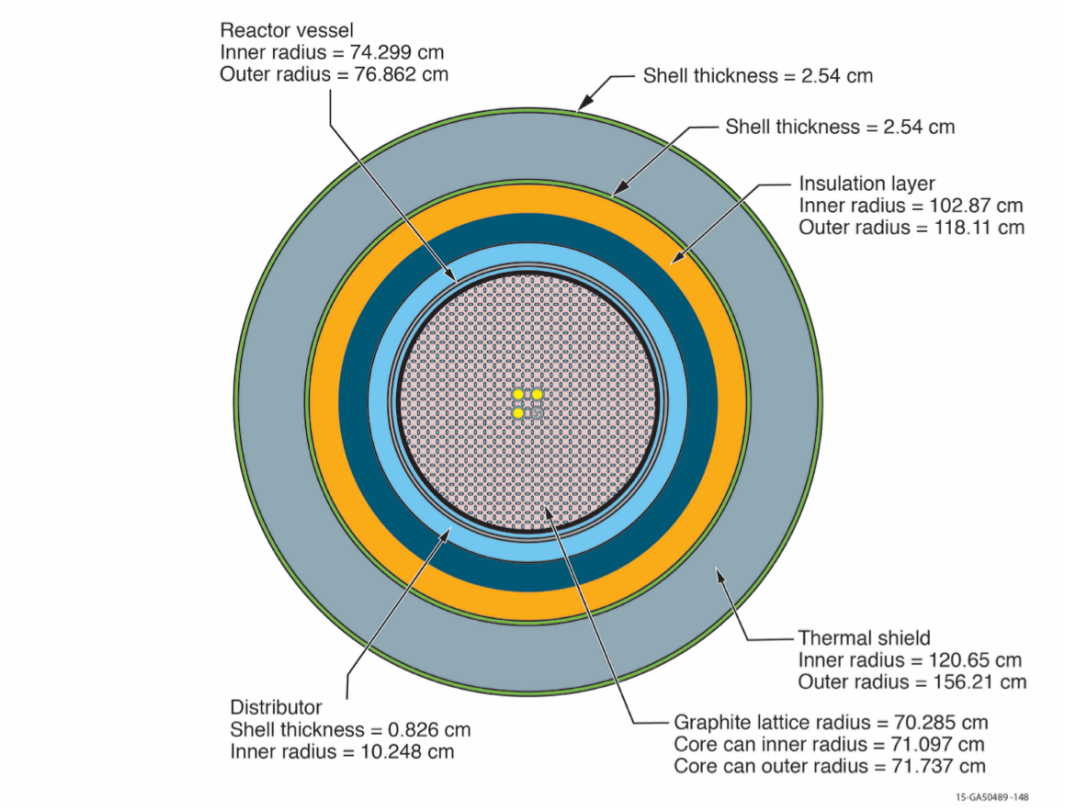

Figure 3.2: Horizontal cross section of the MSRE model at 638 °C. The cross section is located at the centerline of the flow distributor ($z = 145.396$ cm in Figure 3.3). Credit: David R. Sharp, Idaho National Laboratory.

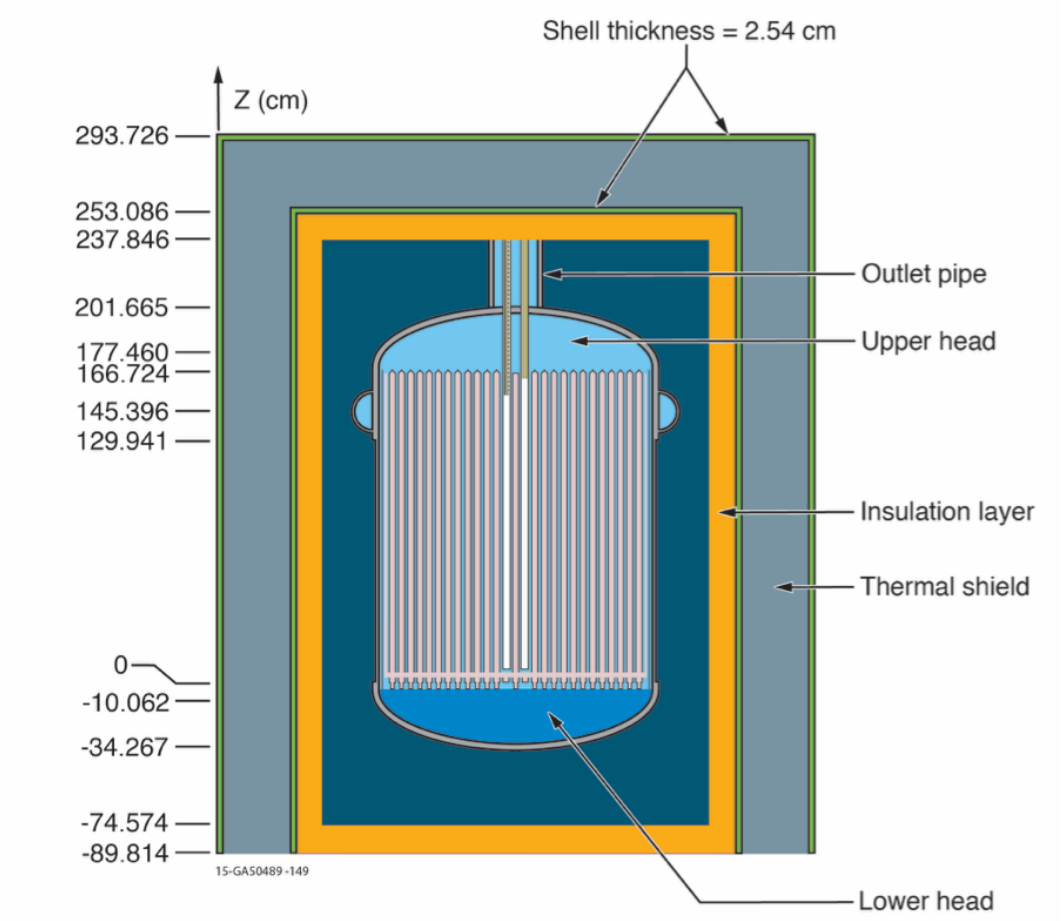

Figure 3.3: Vertical cross section of the MSRE model at 638 °C. The cross section is offset by 5.083 39 cm from the center of the graphite stinger lattice in order to show control rods. Location $z = 0$ corresponds to the bottom of the horizontal graphite lattice. Credit: David R. Sharp, Idaho National Laboratory.

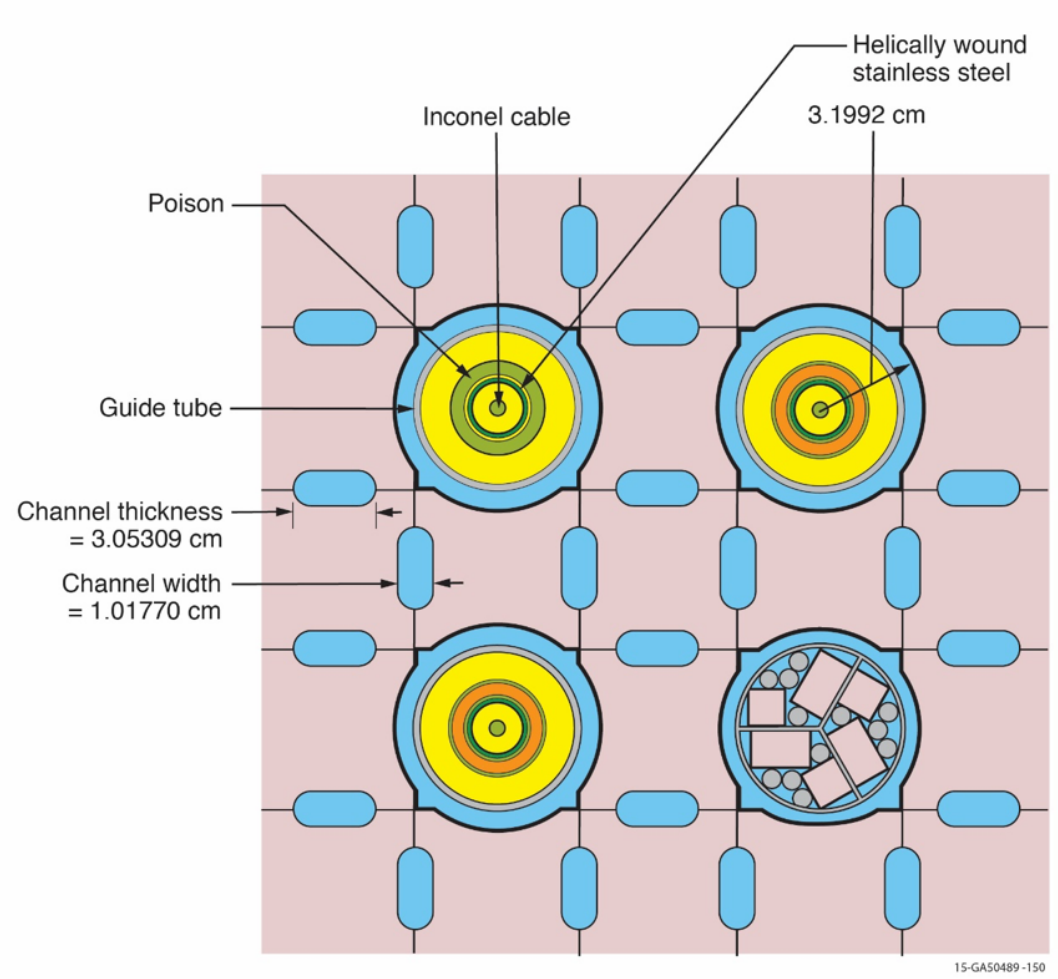

Figure 3.4: Horizontal cross section of control rods and the sample basket at 638 °C. Credit: David R. Sharp, Idaho National Laboratory.

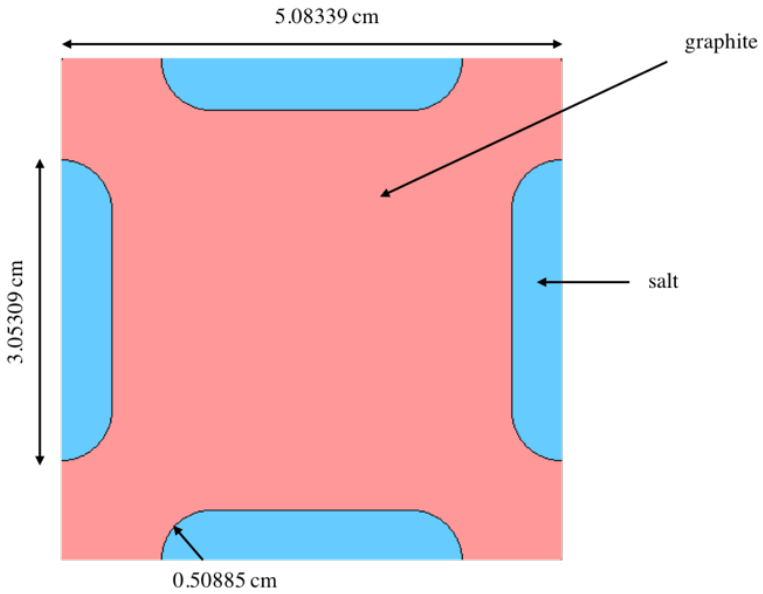

Figure 3.5: Horizontal cross section of single graphite stringer.

to MSRE drawings and blueprints.

At the top of the graphite stringers, a centering bridge (as shown in Figure 2.3 and Figure 2.4) holds two rows of stringers at right angles to each other and these two rows of stringers are higher than regular ones. This centering bridge that helps to prevent shifting of the entire stringer assembly was modeled in detail as shown in Figure 3.7.

Detail dimensions of each component of the core are provided in the official MSRE benchmark specification which was released with the 2019 IRPhEP handbook.

3.2 Materials

As stated before, the MSRE fuel salt was comprised of three parts: (1) the carrier salt, containing the beryllium, zirconium and most of the lithium fluorides; (2) depleted uranium eutectic (73LiF-27UF_4), with the following uranium composition 0.00 % ^{234}U, 0.22 % ^{235}U, 0.00 % ^{236}U, 99.78 % ^{238}U; and (3) highly-enriched uranium eutectic (73LiF-27UF_4), with the following uranium composition 0.95 % ^{234}U, 92.95 % ^{235}U, 0.39 % ^{236}U, 5.70 % ^{238}U. Reference [8] provides the chemical composition of the MSRE fuel salt after calibration according to comparisons between the nominal salt isotopic composition and the results of mass spectrometric analyses, as shown in Table 3.2. According to [8], only 89.07 % of the fuel salt was transferred into the primary loop (this part was referred to as the loop charge) and the rest of the salt remained in the drain tank.

The fuel salt composition at the time of criticality was calculated as 64.88LiF-29.27BeF_2-5.06ZrF_4-0.79UF_4 (expressed as mole percent) from Table 3.2. Reference [8] provides the isotopic composition of uranium in the MSRE fuel salt during initial loading operation, as shown in Table 3.3. ^{7}Li enrichment was 99.995 %. The tolerance range for ^{6}Li enrichment in the salt was between 0.004 % and 0.006 %.

According to [3], at the time of criticality the density of fuel salt was (2.3275 ± 0.0160) g/cm^3 and the mass fraction of ^{235}U in the salt was (1.408 ± 0.007) wt %. The calculated mass fraction of ^{235}U in the salt from the above salt compositions is 1.409 wt % (as shown in Table 3.4) and it agrees well with the tolerance range provided in [3].

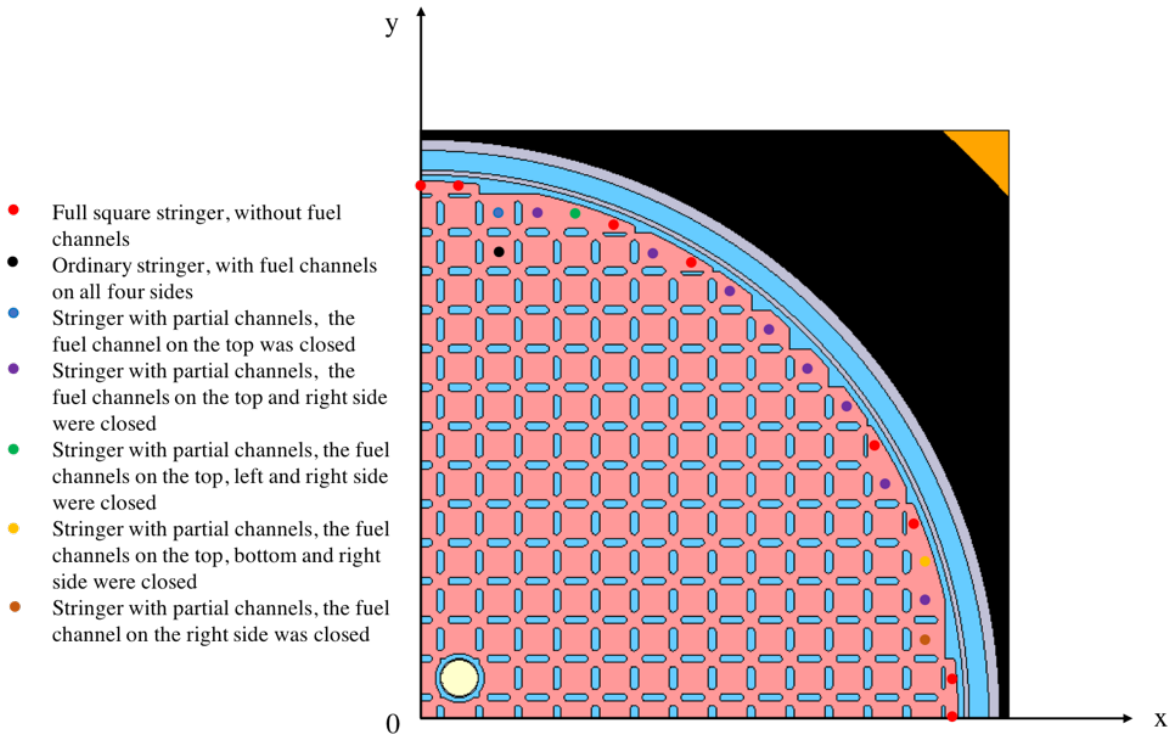

Figure 3.6: Horizontal cross section of 1/4 of the graphite lattice region at $z = 50\,\text{cm}$. The size of the stringers at the edge is determined by a cylinder with center corresponding to the center of the core and a radius of 70.285 cm.

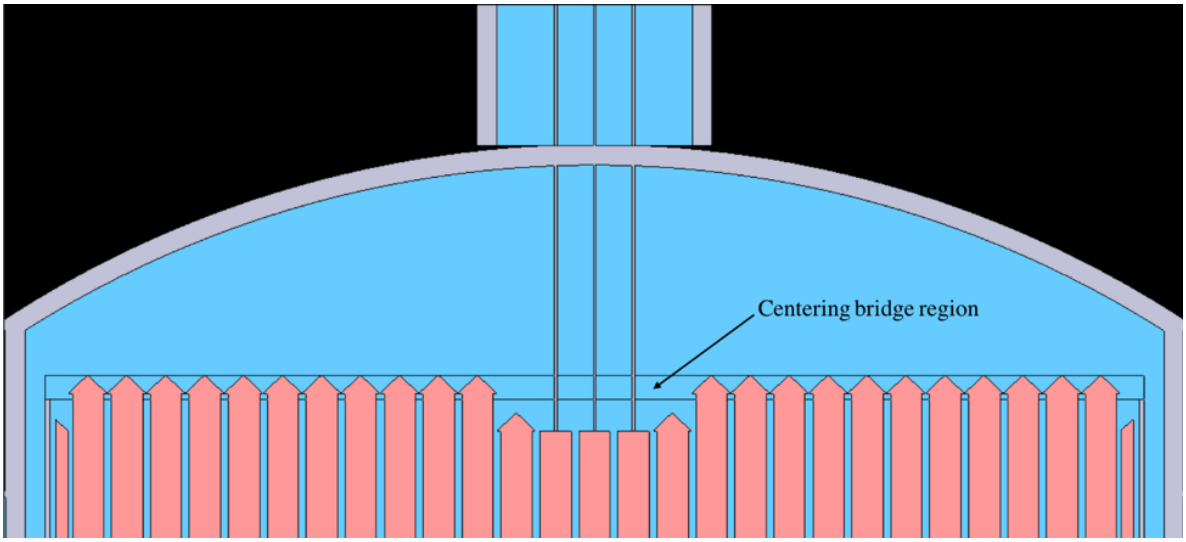

Figure 3.7: Vertical cross section of the MSRE core at $y = 0$, zooming in the centering bridge region.

Table 3.2: Chemical composition of the MSRE fuel salt [8].

Salt type	Li	Be	Zr	U	Sum
Carrier salt, kg	519.16	309.62	541.36	0.0	4520.0
Depleted uranium eutectic, kg	11.55	0.	0.0	145.60	234.5
Highly-enriched uranium eutectic, kg	5.84	0.	0.0	73.59	118.55
Total fuel salt, kg	534.30	309.62	541.36	219.19	4873.05
Loop charge (89.07 %), kg	475.90	275.78	482.19	195.23	4340.43

Table 3.3: Isotopic composition of uranium in the MSRE fuel salt during initial loading operation [8].

Event	Total U, kg	^{234}U, kg	^{235}U, kg	^{236}U, kg	^{238}U, kg
Loading of depleted uranium eutectic	145.600	0.000	0.323	0.000	145.277
Additions of highly-enriched eutectic on May 25, 1965	47.490	0.452	44.143	0.187	2.708
Additions of highly-enriched eutectic on May 30, 1965	26.100	0.249	24.261	0.102	1.488
Total in the detail tank (before charge)	219.190	0.701	68.727	0.289	149.473
Loop charge (89.07 %)	195.233	0.624	61.215	0.257	133.136

Table 3.4: Mass fraction of uranium isotopes in the MSRE fuel salt at the time of criticality.

Isotope	^{235}U	^{234}U	^{236}U	^{238}U
Mass fraction in total salt, wt.%	1.409	0.014	0.006	3.065

Table 3.5: Concentration of impurities in the MSRE fuel salt [8].

Element	Concentration, ppm
Fe	162
Cr	28
Ni	30
O	490

The concentration of impurities of fuel salt is provided in Table 3.5. According to [11], the primary corrosion mechanism in the MSRE fuel salt system was selective removal of chromium by:

$$2\,UF_4 + Cr(\text{in alloy}) \rightleftharpoons 2\,UF_3 + CrF_2(\text{in salt})$$

and the concentration of chromium in salt serves as the primary indicator of corrosion.

The zirconium tetra-fluoride used for the MSRE fuel salt was essentially hafnium free (< 50 ppm Hf). In addition to the impurities provided in Table 3.5, it was postulated that undissolved helium could be present if entrained in the circulating fuel through the action of the fission product gas stripping device. Nevertheless, a gamma-ray densitometer positioned on the reactor inlet line detected no measurable helium void. The sensitivity of the void measurement was 0.076 vol$\%$ [12]. The expansion coefficient of the fuel salt is $-1.18 \times 10^{-4}\,{}^{\circ}F^{-1}$.

The salt-containing piping and equipment are made of INOR-8, a special high-nickel and molybdenum alloy having a good resistance to attack by fuel and coolant salts at temperatures at least as high as 816 °C. The density of INOR-8 is 8.7745 g/cm^3 with the nominal composition of 68%Ni-17%Mo-7%Cr-5%Fe.

The graphite for the MSRE is a special grade, given the designation "CGB" by the National Carbon Company. The designed properties of the MSRE graphite are listed in Table 3.6. Reference [13] evaluated the as-built MSRE graphite and found that the bulk density ranged from 1.83 g/cm^3 to 1.87 g/cm^3, with an average value of 1.86 g/cm^3. The CGB graphite is a new material of high density and small pore size at the time of the MSRE experiments. The fuel salt does not wet the graphite and therefore should not enter the pores, even at pressure well above the operating pressure. Extremely small quantities of salt may penetrate the graphite either through pores or cracks and there is <2 g of uranium in the 3.700 kg of graphite in the entire core after 2.5 years exposure in the MSRE fuel salt [2]. The MSRE graphite was expected to release the oxygen in the form of water vapor during the planned pretreatment [13]: the graphite was carefully heated in dry helium to desorb water vapor after installation in the reactor and a purge salt was thoroughly circulated through the primary system to remove all but trace amounts of oxygen before any fuel salt was introduced. The graphite core lattice is sufficiently unrestrained and the coefficient of thermal expansion is provided in Table 3.7.

3.3 Modeling of reactivity effect experiments

The geometry arrangements of the benchmark model for determination of the reactivity effects measurements are identical to those of the first zero-power critical core configuration described above with the exception of the control rod position and temperature. The reactivity effect experiment was operated at 649 °C, rather than 638 °C (the temperature for the criticality experiment). Therefore, the dimensions of the reactivity benchmark model differ from the criticality benchmark model but simplifications applied to both models remain the same. Novel methods were developed to model required characteristics and experimental parameters in the MSRE model as follows.

Table 3.6: Properties of MSRE core graphite - CGB [6].

Property	Value
Bulk density, g/cm^3	1.83 to 1.89
Salt absorption at 150 psig, vol%	0.20
Ash, wt %	0.0005
Boron, wt %	0.000 08
Vanadium, wt %	0.0009
Sulfur, wt %	0.0005
Oxygen, cm^3 of CO(STP) per 100 cm^3 of graphite	6.0

Table 3.7: Thermal expansion coefficient of the graphite and INOR-8 in the 70 °F to 1200 °F range [6].

Material	Coefficient of thermal expansion, °F^{-1}
Graphite	1.3×10^{-6} to 1.7×10^{-6}
INOR-8	7.8×10^{-6}

3.4 Control rod worth

The three control thimbles are centered at (5.083 39 cm, 5.083 39 cm), ($-$5.083 39 cm, 5.083 39 cm) and ($-$5.083 39 cm, $-$5.083 39 cm) as shown in Figure 3.8, regarding the center of the graphite lattice as the origin. Each control rod element is modeled as a cylinder with a flat surface at the top and bottom closures (see Figure 3.9). Control rod elements are packed vertically inside each control rod thimble.

To calculate the differential and integral control rod worth, rod No. 1 (the upper right one shown in Figure 3.8) was moved $\pm\Delta x$ cm from specified configurations to obtain the difference of reactivity from the difference of rod positions. Control rod No. 2 and No. 3 are withdrawn to the upper limit at this moment and the differential worth of rod No. 1 at position x was calculated applying the following equation:

$$f(x) = \frac{\rho(x + \Delta x) - \rho(x - \Delta x)}{2\Delta x} \tag{3.1}$$

Due to the complex shape of the control rod elements and the way they were threaded in the stainless steel tube, it would be time-consuming to write new Serpent 2 input every time with a change of parameter related to control rods. A Python script was developed to automatically generate the Serpent 2 input with user-specified rod-related parameters such as rod position and temperature. Also, given a predefined bottom position of the poison part and Δx, the step of vertically moving distance, the Serpent 2 inputs with control rod No. 1 moving from the top to the bottom of the control rod thimble can be generated, as shown in Figure 3.10.

3.5 Reactivity coefficient of ^{235}U concentration

The reactivity coefficient of ^{235}U concentration is defined as the ratio of change in reactivity to the fractional change in ^{235}U loadings in loop while holding the control rods still and it can be obtained from:

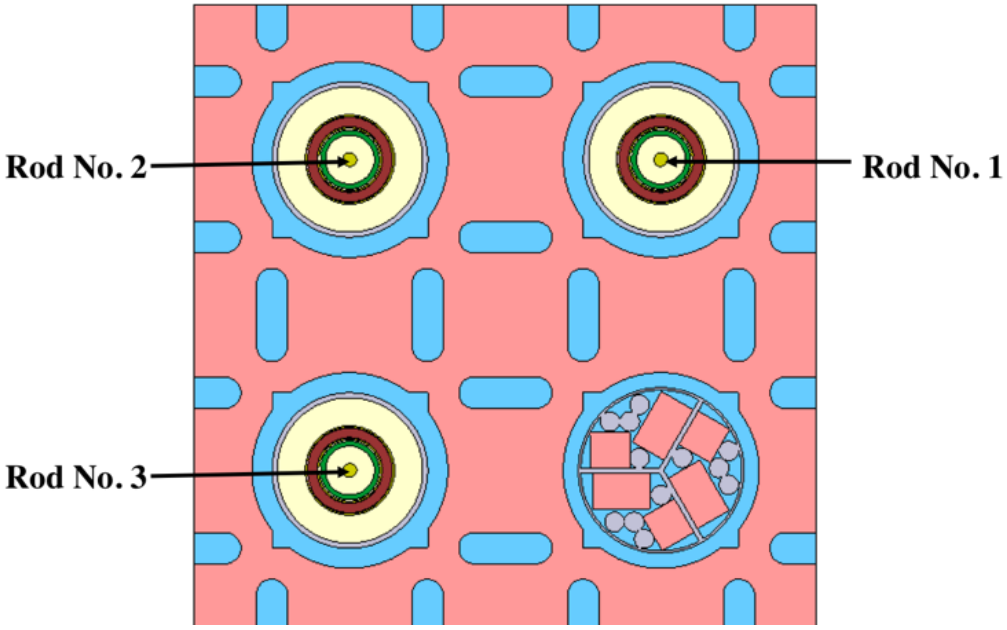

Figure 3.8: Horizontal cross section of three control rods, rod No. 1 is the regulating rod and rod No. 2 and 3 are the shim rods.

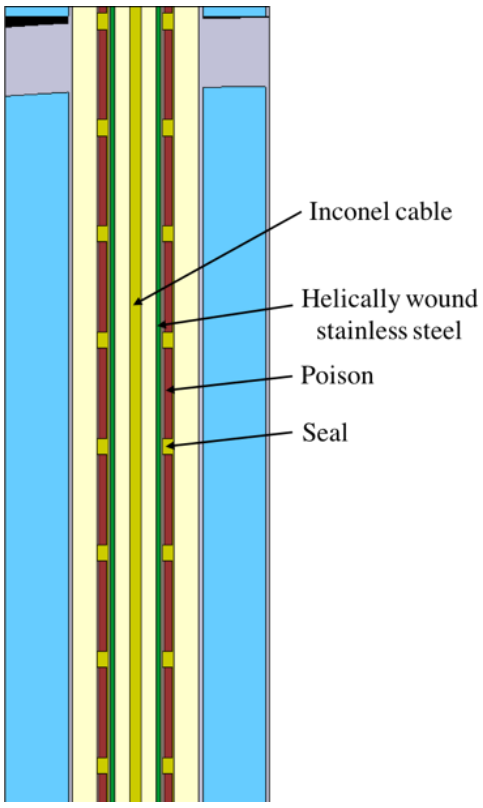

Figure 3.9: Vertical cross section of the control rod in the Serpent 2 model.

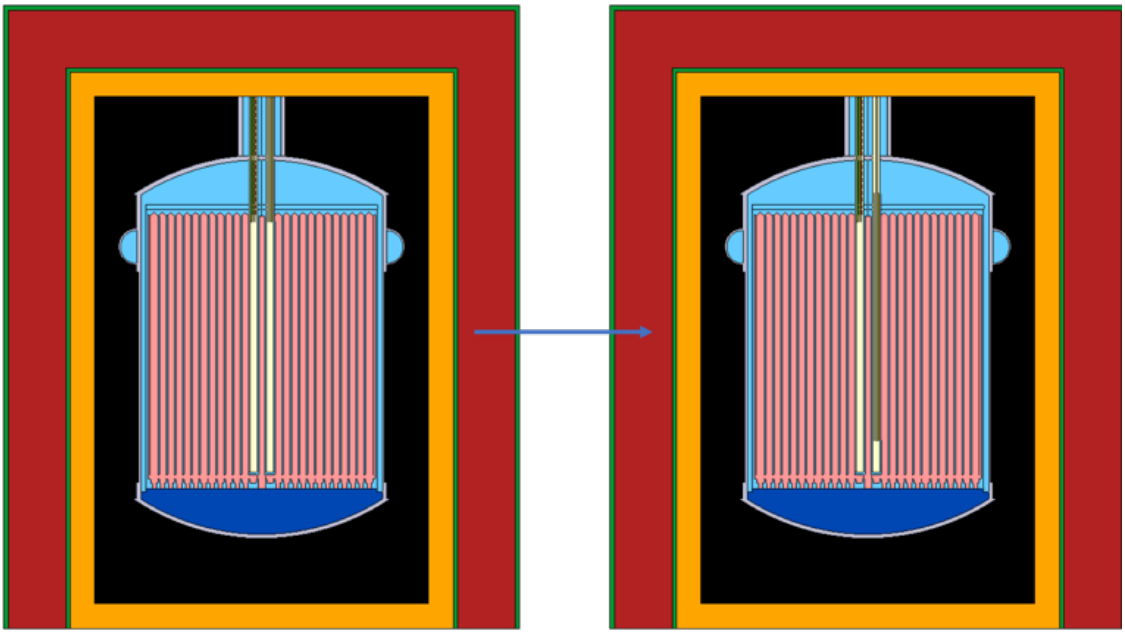

Figure 3.10: Vertical cross section of the control rods, moving rod No. 1 from 51 in (the top) to -2 in (the bottom), inch was the unit of length to describe control rod travel as in [3].

$$\Delta\rho = \frac{K(C - C_0)}{C} \tag{3.2}$$

where C is the loadings of ^{235}U in the salt, C_0 is the value at the minimum critical loading which is 65.25 kg, and K is the reactivity coefficient of ^{235}U concentration.

To obtain the reactivity coefficient of ^{235}U concentration, reactivity for cases with various ^{235}U loadings in the loop and the same control rod position was calculated (the core configuration was set as all control rods withdrawn to their upper limit). If the assumption recognized by ORNL experimenters, that the reactivity coefficient of ^{235}U is nearly independent of ^{235}U mass over the range during the experiment [3], holds true, the average value of this reactivity coefficient can be obtained as the linear regression coefficient as shown in Figure 3.11.

It was found that the accuracy of this calculation relied heavily on the knowledge of fuel salt composition, with certain amount of excess ^{235}U addition for every calculation step. The initial composition of the fuel salt in loop for the rod calibration experiments is listed in Table 3.8 and this composition was calculated by applying a factor of 94.94 % to the total fuel salt composition listed in Table 3.2 to make the ^{235}U loading in loop equal to 65.25 kg, the value specified in [3] as the minimum critical loading. The control rod calibration experiments were performed right after the first zero-power criticality experiment and the reason for the discrepancy between the loop charge of ^{235}U listed in Table 3.2 and the reported value of 65.25 kg in [3] is due to some unknown reasons. This discrepancy won't affect the salt composition used in the criticality benchmark since the total density of salt is settled. However, the control rod calibration experiments are very sensitive to this parameter since the total volume of salt starts to have an impact with excess ^{235}U added. To agree better with the control rod calibration experiments, the value of 65.25 kg for the initial loading of ^{235}U was accepted. Also, with this total ^{235}U in the loop and the corresponding total salt mass of 4626.52 kg in the loop, the total salt volume in the loop was then calculated to

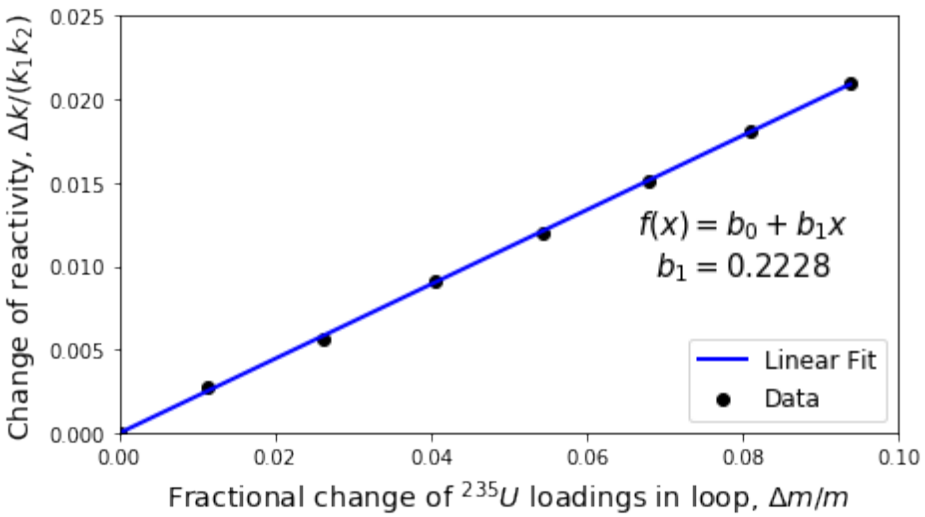

Figure 3.11: Effect of ^{235}U mass on reactivity.

Table 3.8: Composition of fuel salt at the beginning of control rod calibration experiment, applying a factor of 94.94 % to the chemical composition of the total fuel salt provided in Table 3.2.

Fuel salt component	Value, kg
Li	507.27
Be	293.96
Zr	513.97
U	208.10
^{234}U	0.67
^{235}U	65.25
^{236}U	0.27
^{238}U	141.91
F	3103.22

be 1.9936 m^3, which agrees well with the reported value of 1.996 m^3 in Table 2.1.

The density of fuel salt at the initial criticality moment was reported as 2.3275 g/cm^3 at 638 °C. Since the fuel salt expansion coefficient is -1.18×10^{-4}/°F, the salt density at 649 °C was calculated to be 2.3223 g/cm^3.

Table 3.9 provides the salt compositions for cases with ^{235}U loading ranging from 65.25 kg to 72 kg in loop. On each step, highly-enriched uranium eutectic (73LiF-27UF_4) was added to exhaust the required ^{235}U loadings. It is assumed that the total salt volume won't be changed significantly during the addition of enriched uranium eutectic and the salt density for each case was calculated by the ratio of salt mass and salt volume.

3.6 Rod-shadowing effect

During the additions of enriching capsules, the change in the critical position of the regulating rod (rod No. 1) was recorded as the shim rods (rods No. 2 and No. 3) were inserted into the core. As shown in Figure 3.12, both the effect of inserting a single shim rod (rod No. 2) with rod No. 3

Table 3.9: Salt composition with various ^{235}U loadings at 649 °C, represented as loadings in kg in the loop.

Case	1	2	3	4	5	6	7	8
Li	507.27	507.33	507.42	507.50	507.59	507.67	507.76	507.85
Be	293.96	293.96	293.96	293.96	293.96	293.96	293.96	293.96
Zr	513.97	513.97	513.97	513.97	513.97	513.97	513.97	513.97
Hf	0.0029	0.0029	0.0029	0.0029	0.0029	0.0029	0.0029	0.0029
U	208.10	208.91	209.98	211.06	212.14	213.21	214.29	215.36
^{234}U	0.67	0.67	0.68	0.69	0.70	0.71	0.72	0.73
^{235}U	65.25	66.00	67.00	68.00	69.00	70.00	71.00	72.00
^{236}U	0.27	0.28	0.28	0.29	0.29	0.29	0.30	0.30
^{238}U	141.91	141.96	142.02	142.08	142.14	142.20	142.26	142.32
Fe	0.75	0.75	0.75	0.75	0.75	0.75	0.75	0.75
Cr	0.13	0.13	0.13	0.13	0.13	0.13	0.13	0.13
Ni	0.14	0.14	0.14	0.14	0.14	0.14	0.14	0.14
O	2.27	2.27	2.27	2.27	2.27	2.27	2.27	2.27
F	3103.22	3103.65	3104.22	3104.79	3105.36	3105.93	3106.51	3107.08
Total	4629.80	4631.10	4632.84	4634.57	4636.30	4638.03	4639.77	4641.50

held fixed in the fully withdrawn position, and the effect of inserting rods No. 2 and 3 as a bank (at identical elevation) were recorded . The 45° line represents the situation where the moved shim rod and the regulating rod were at equal position.

This experiment was not incorporated into the MSRE benchmark due to lack of experimental uncertainty information and difficulty to be reproduced accurately. The strategy to make a preliminary code-to-experiment comparison is provided here.

1. The banked critical positions of rod No. 1, 2 and 3 (all three control rods were inserted together at identical positions) while total ^{235}U loading in loop was 67.94 kg, 69.94 kg and 71.71 kg were measured to be 39.0 in , 33.3 in and 28.4 in from Figure 3.12. The k_{eff} for these three cases were calculated and regarded as the baseline k_{crit} for these three levels of ^{235}U concentration. The reason behind this approach is that the k_{eff} yielded by the benchmark model is biased from unity and this bias may not be constant with different ^{235}U loadings in the system.

2. The objective is to calculate the critical position of the shim rods for each data point in Figure 3.12 while the position of rod No. 1 was set the same as in the figure.

3. For each data point with a certain ^{235}U level and rod No. 1 position, the k_{eff} of two cases with the shim rods set with 2 in apart, surrounding the potential critical position, were calculated.

4. Calculate the critical position of the shim rods by linearly interpolation from the data obtained from the previous step, as shown in Figure 3.13.

5. For each data point, check the k_{eff} obtained from the calculated critical shim rods position to make sure the difference between k_{eff} (calculated) and certain k_{crit} (the baseline) is within 20 pcm. Otherwise, repeat from step 2.

3.7 Drift of delay neutron precursors

As discussed in [14], an important phenomenon that is typical of circulating fuel reactors is the drift of DNPs and the consequent effect on reactivity. As fuel circulates in and out of the core relatively rapidly, DNPs drift from the fission location to a new location, inside or outside of the core, before releasing a neutron. Typically, this corresponds to a loss in reactivity as delayed neutrons are either emitted outside of the core, thus, are lost, or in the core, but in a lower importance region, i.e., closer to the core periphery.

In the MSRE the reactivity impact of salt circulation was first evaluated during the initial campaign of zero-power criticality experiments by determining the difference in the required load of ^{235}U in order to make the reactor critical with the fuel salt stationary and circulating. It was found that following the initial critical experiment with fuel salt stationary, when the salt pumping was activated another 8 capsules containing 85 g ^{235}U each were needed to be added to the loop to return the system critical. The reactivity loss due to fuel salt circulation was then estimated to be (-212 ± 4) pcm, given by the vertical difference between the curves in Figure 3.14.

The assessment of reactivity change due to fuel motion was replicated using the benchmark model. However, the base model was slightly modified as shown in Figure 3.15. The distributor was removed and the shape of the vessel was changed to a cylinder while keeping the volume of the upper head and lower head unchanged. Such modification supports the assumption of a flat velocity profile for the salt through each region and it is not expected to significantly impact the results of the assessment.

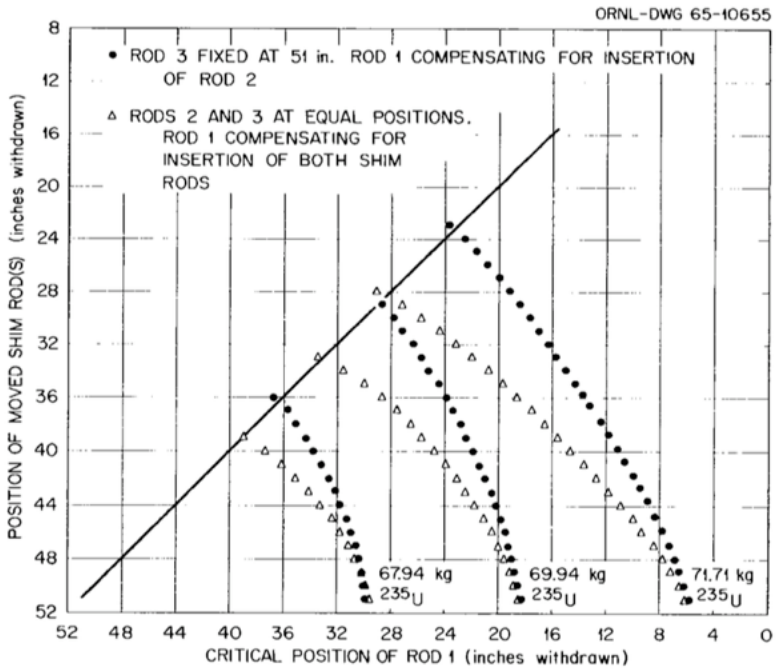

Figure 3.12: Change in critical position of rod No. 1 as shim rods No. 2 and 3 are inserted into the core [3].

The main impact of salt circulation on reactivity is due to a change in the effective delayed neutron fraction, β_{eff}. In order to obtain β_{eff} for the circulating case, the following considerations are made. The ratio between β_{eff} with circulating and stationary salt can be determined as follows [15]:

$$\frac{\beta^c_{eff}}{\beta^s_{eff}} = \frac{\int_{core} D^c(\vec{r}) I^c(\vec{r}) dV}{\int_{core} D^s(\vec{r}) I^s(\vec{r}) dV} \tag{3.3}$$

where $D(\vec{r})$ is the probability density for DNPs to decay in position $\vec{r}$, and $I(\vec{r})$ is the spatial dependence of the neutron importance. β_{eff} can be calculated through the following equation where k_p is the multiplication factor for prompt neutrons only, which is the same in the circulating and the stationary salt case because prompt neutrons do not flow with the fluid:

$$\beta_{eff} \simeq 1 - \frac{k_p}{k_{eff}} \tag{3.4}$$

Given k_{eff} and β_{eff} in the stationary salt case, k_{eff} in the circulating case is obtained combining Eq. 3.3 and Eq. 3.4. $I(\vec{r})$, $D^s(\vec{r})$ and $D^c(\vec{r})$ are determined as in Eq. 3.5, Eq. 3.6 and Eq. 3.7, respectively. It is assumed that the neutron importance function is the one for a bare, cylindrical core. R_e and H_e represent extrapolated radius and height of the core, respectively. In the stationary case DNPs decay where they are generated, therefore, D^s resembles the fission power distribution. The radial dependence of the fission rate distribution is assumed in the shape of J_0 Bessel function. The axial distribution is obtained as a product of the ratio of fuel salt volume to total volume $\alpha(z)$, and the linear fission rate in the fuel salt $f(z)$ calculated using the simplified MSRE model discussed above. In the case of circulating fuel (Eq 3.7), the DNP drift is accounted

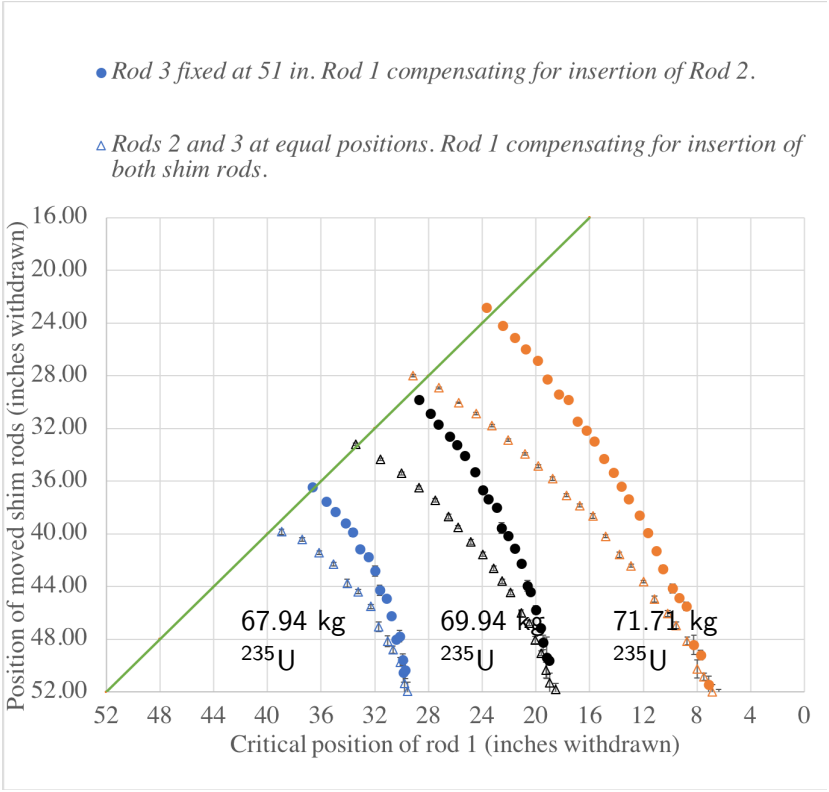

Figure 3.13: Calculated change in critical position of rod No. 1 as shim rods No. 2 and 3 are inserted into the core.

for by introducing the term $P(z', z)$ that is the probability for a DNP created in z' to decay in z as determined by the DNP decay constant λ, and the salt's speed v (Eq. 3.8). Furthermore, since not all DNPs decay within their first loop an additional term is necessary (Eq. 3.7) where $P_{null}(z)$ represents the probability for a DNP born in z does not decay during the first loop, and T is the total time the salt requires for each loop. It is assumed that DNPs perfectly mix before reentering the core, and at the core entrance are evenly distributed over the radial location.

$$I(r, z) = J_0(\frac{2.405r}{R_e})cos(\frac{\pi z}{H_e}) \tag{3.5}$$

$$D^s(r, z) = J_0(\frac{2.405r}{R_e})\alpha(z)f(z) \tag{3.6}$$

$$D^c(r, z) = [\int_{-H/2}^{z} \alpha(z')f(z')P(z', z)dz']J_0(\frac{2.405r}{R_e})+ \frac{\int_{-H/2}^{H/2} \alpha(z')f(z')P_{null}(z')dz' \int_0^R J_0(\frac{2.405r}{R_e})2\pi r'dr'}{\pi R^2} \times P(-H/2, z) \times \frac{e^{\lambda T}}{e^{\lambda T} - 1} \tag{3.7}$$

$$P(z_1, z_2) = exp(-\lambda t(z_1, z_2))\frac{\lambda}{v(z_2)} \tag{3.8}$$

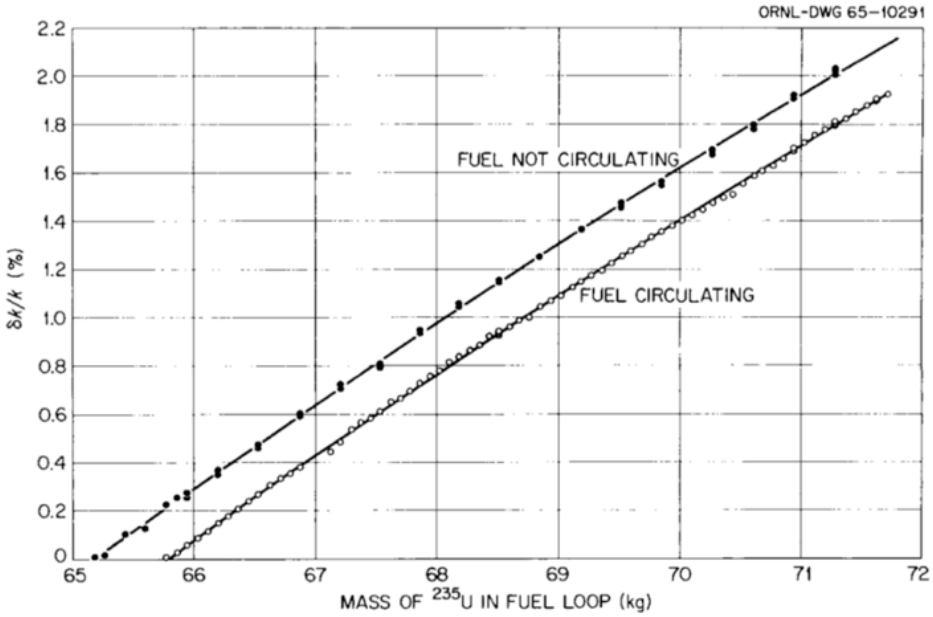

Figure 3.14: Effect of ^{235}U mass on reactivity with and without fuel circulating [3].

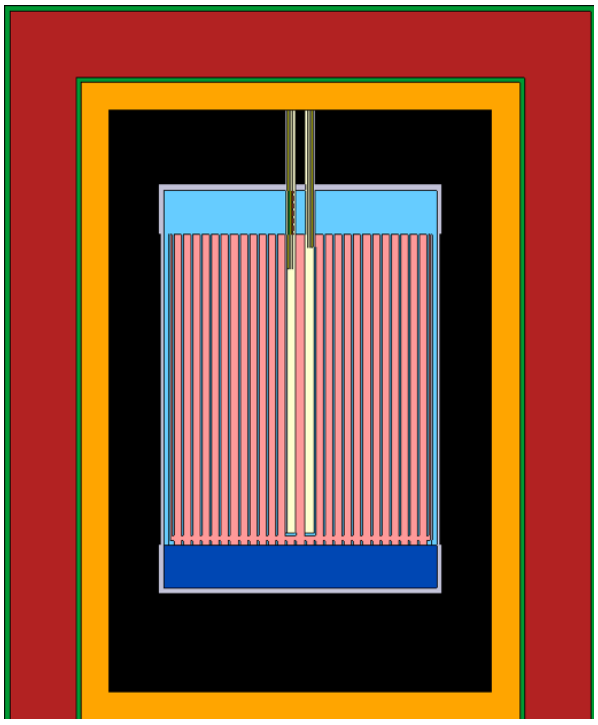

Figure 3.15: Vertical cross section of the simplified MSRE model used to calculate the reactivity effect of fuel salt circulation.

3.8 Rod-drop effect

In rod-drop experiments, the position of the fission chambers was adjusted to obtain an initial count rate at criticality of ∼30 000 counts/s. The MSRE instrument shaft was placed remotely relative to the reactor core (see Figure 2.12), minimizing errors due to changes in the spatial flux shape during the rod-drop experiment. Hence, the theoretical time-integrated flux following the rod-drop can be obtained by solving the standard space-independent reactor kinetics equations [3]:

$$\frac{d\psi}{dt} = n(t) \tag{3.9}$$

$$\frac{dn(t)}{dt} = \frac{\Delta\rho(t) - \beta}{\Lambda} n(t) + \sum_{i=1}^{6} \lambda_i C_i(t) \tag{3.10}$$

$$\frac{dC_i(t)}{dt} = \lambda_i C_i(t) + \frac{\beta_i n(t)}{\Lambda}, i = 1, 2, ..., 6 \tag{3.11}$$

where

- $\psi(t) =$ time-integrated count rate following the scram,
- $n(t) =$ detector count rate following scram,
- $C_i(t) =$ DNP concentrations, normalized to detector count rate,
- $\Delta\rho(t) =$ reactivity addition vs time following scram,
- $\beta_i =$ production fraction for $i - th$ group of delayed neutrons,
- $\lambda_i =$ radioactive decay constant for $i - th$ group precursors,
- $\Lambda =$ prompt neutron generation time.

The initial conditions are:

$$\psi(0) = 0, \tag{3.12}$$

$$n(0) \sim 30,000 \text{ counts/s, initial count rate at critical condition,} \tag{3.13}$$

$$C_i(0) = \frac{\beta_i n(0)}{\Lambda \lambda_i} \tag{3.14}$$

The time variation of the reactivity is governed by:

$$\Delta\rho(t) = \rho(y_0) - \rho[y(t)] \tag{3.15}$$

$$\begin{aligned} y(t) &= y_0, && 0 \le t \le t_e \\ &= y_0 - \frac{1}{2} a t^2, && t_e \le t \le t_e + t_m \\ &= y_s, && t_e + t_m \le t \end{aligned} \tag{3.16}$$

where

$y =$ rod position; initial critical position, y_0; scram position, y_s,

$\rho(y) =$ magnitude of reactivity worth corresponding to rod position y,

$t_e =$ effective lag time between scram signal and start of rod drop, $\sim$20 ms,

$a =$ acceleration during rod fall ($\sim$15 ft/s^2, basing on drop-time measurements on the MSRE control rods made during pre-nuclear testing [3]),

$t_m =$ time to fall to scram position.

Applying the integral worth curve $\rho(y)$ of different rod group and ^{235}U loadings, after a certain amount of capsules of enriching salt was added, and β_{eff} calculated from the MSRE Serpent 2 model, the integrated count rate curve can be obtained by a Python script to solve these equations above. This experiment is not covered in the MSRE benchmark due to lack of experimental uncertainty information. But a preliminary code-to-experiment comparison can be made following the strategies described above.

Results

4.1 Multiplication factor

4.1.1 Code-to-experiment validation

The experimental k_{eff} for the MSRE first criticality experiment was unity. The assessed bias of the benchmark model (described in Chapter 3) from simplifications is -22 pcm; therefore, the expected k_{eff} for the benchmark model is 0.999 78.

The MSRE was modeled with the Monte Carlo code Serpent 2 (version 2.1.30 [16]), using the ENDF/B-VII.1 cross-section library. The temperature for cross section library is set at 900 K (627 °C) and it is pre-processed for Doppler broadened to 911 K (638 °C) by Serpent 2. The thermal scattering library is based on ENDF/B-VII.0 for C in graphite, with temperature 911 K (638 °C) in the core and 305 K (32 °C) in the thermal shield, and H in water, with temperature 305 K in the thermal shield. For thermal scattering, Serpent 2 applies temperature interpolation among the two closest temperature libraries. The Serpent 2 model of the first criticality experiment of the MSRE with ^{235}U yielded an effective multiplication factor of 1.021 32, with a standard deviation (1σ) of 0.000 034.

The calculated k_{eff} is 2.154 % larger than the experimental and benchmark model value. The complexity of the model makes it difficult to identify the source(s) of such discrepancy. The model was reconstructed based on the public available documents more than 50 years after the experiment. It can be noticed that k_{eff} is particularly sensitive, as obvious, to the main core components that are salt and graphite. Salt composition is particularly challenging to determine as obtained by successive addition. Changes in salt composition would largely impact k_{eff}. At the time the benchmark was prepared, thermal scattering kernel data for salt was not available, although the impact of that is expected to be smaller than the observed difference.

The accuracy of reactor neutronics calculations is sensitive to which nuclear data library was used. It was found that the use of JENDL-3.3 (Japan), compared to ENDF (US) and JEFF (Europe), yielded the k_{eff} for the HTTR (a graphite-moderated, helium-cooled reactor) criticality calculations with the best accuracy (as shown in Table 4.1), which are mainly caused by the slight difference in the neutron capture cross section of carbon at 0.0253 eV among the libraries [17].

According to [17], the neutron capture cross section of carbon at 0.0253 eV was revised based on the latest measurement data in JENDL-4.0 and the discrepancies between the experimental and calculation results of HTTR were further decreased using JENDL-4.0.

The use of ENDF/B-VII.1 vs. JENDL-4.0 cross section for the MSRE critical model led to a difference of (71 ± 5) pcm in k_{eff}, as shown in Table 4.2. In addition, it was found that the eigenvalue for the MSRE core calculated using ENDF/B-VII.1 data would be decreased by (178 ± 5) pcm if only the carbon cross section was replaced by JENDL-4.0 data. The use of JENDL-4.0, especially the carbon cross section, can improve the accuracy of the MSRE calculation but the discrepancy is still around 2 %.

Actually, for benchmarks of a carbon-enriched system, Monte Carlo codes tend to overestimate the k_{eff} of the benchmark model by 1 % to 2 %, as shown in Table 4.3. The bias is possibly due to

Table 4.1: Results for the HTTR benchmark model evaluation of the fully-loaded core critical, all values from the IRPhEP benchmark (HTTR-GCR-RESR-001) and obtained with the Monte Carlo code MCNP.

Neutron cross-section library	Expected k_{eff}	Calculated k_{eff}	(C-E)/E
ENDF/B-V.2	1.0025	1.0198±0.0001	1.72
ENDF/B-VI.8	1.0025	1.0222±0.0001	1.96
ENDF/B-VII.0	1.0025	1.0229±0.0001	2.03
JEFF-3.1	1.0025	1.0236±0.0001	2.10
JENDL-3.3 with ENDF/B-VII.0 S(α, β)	1.0025	1.0178±0.0001	1.53

Table 4.2: Expected and calculated benchmark-model k_{eff} values.

Code (Data library)	Calculated k_{eff}	Benchmark k_{eff}	100(C-E)/E
Serpent 2 (ENDF/B-VII.1)	1.02132±0.000034	0.99978±0.00420	2.154
Serpent 2 (JENDL-4.0)	1.02061±0.000034	0.99978±0.00420	2.083

uncertainties in the impurity content of the graphite blocks, the accuracy of the neutron capture cross section of carbon and the accuracy to model the nuclear-grade graphite.

4.1.2 Experimental uncertainty analysis

The experimental uncertainty of k_{eff} is the uncertainty caused by experimental parameters. To determine the uncertainty from each parameter, k_{eff} is calculated perturbing one parameter at a time within its uncertainty range, in both positive and negative directions. Δk_i is obtained as follows, assuming that the change of k_{eff} is in proportion to the change of parameter i:

$$\Delta k_i = \frac{u_i}{\delta x_i}(k_{\delta_i} - k_{ref}) \tag{4.1}$$

where u_i is the standard uncertainty of parameter i, and $(k_{\delta_i} - k_{ref})$ is the change in k_{eff} induced by change δx_i on parameter i. When there is a difference between the absolute values of

Table 4.3: Difference between calculated k_{eff} and expected k_{eff} for selected full-core benchmarks with carbon-enriched system, all values from the IRPhEP handbook.

Benchmark model	Code (data library)	Expected k_{eff}	Calculated k_{eff}	100(C-E)/E
HTR10 high-fidelity	MCNP (ENDF/B)	1.00000	1.01190±0.00021	1.190
HTR10 simplified	MCNP (ENDF/B)	1.0131	1.02500±0.00021	1.175
HTTR fully-loaded	MCNP (END/B-VII.0)	1.0025	1.02310±0.00010	2.03
PROTEUS Core 3	MCNP5 (ENDF/B-VII.0)	0.9999	1.00888±0.00007	0.90

Δk_i calculated from positive and negative perturbations of a parameter, the larger Δk_i is selected, as shown in Table 4.4. For this evaluation, all parameters are considered uncorrelated. To hold this assumption true, for example, when perturbing ^{235}U, ^{234}U and ^{236}U mass fraction in the fuel salt, ^{238}U mass fraction was adjusted accordingly to compensate any mass fraction change and in this way, the uncertainty of k_{eff} from ^{238}U mass fraction uncertainty does not have to be calculated separately to avoid correlation. The total standard uncertainty of k_{eff} is the root mean square of all Δk_i.

The (1σ) uncertainty of the experimental k_{eff} was then calculated to be 420 pcm, as shown in Table 4.4. The graphite density, ^{6}Li enrichment and fuel salt density are the most important uncertainty contributors.

4.1.3 Further discussions of k_{eff}

As discussed before, the accuracy of Monte Carlo calculations for nuclear reactor neutronics analysis is sensitive to the cross section library including the thermal scattering library used for graphite which is especially important to the MSRE. The effect of different thermal scattering cross section temperatures was evaluated by Serpent 2 as shown in Table 4.5. The thermal scattering library is based on ENDF/B-VII.0. It was found that a 100 K change in temperature of thermal scattering cross section of carbon in graphite will result in more than 500 pcm difference in k_{eff}.

The detailed fuel salt composition at the critical point of the MSRE zero-power experiment remains mysterious until a thorough investigation to the fuel salt preparation was conducted, mainly basing on the technique report describing the chemical behaviour in the fuel salt during pre-nuclear operations [8]. The benchmark salt composition is chosen as the nominal salt composition provided in [8] that recorded how much salt component was put into the primary loop and this composition was checked and corrected by the experimenters to be self-consistent. There are two other reference salt compositions: one is from the chemical analyses performed with samples of the fuel salt during the experiment; another one is in the form of anticipated mole fraction of the fuel salt (65.0LiF-29.17BeF_2-5.0ZrF_4-0.83UF_4 [8]), which is close to the fuel salt composition specified or expected for MSRE power operation provided in [3] (65LiF-29.2BeF_2-5ZrF_4-0.8UF_4). All of these salt options were evaluated on the benchmark model (as shown in Table 4.6), keeping the enrichment of all uranium isotopes, impurities concentration and total salt density the same.

It was found that the result from chemical analyses shows bias in determination of lithium and beryllium when compared with the other two. Actually similar measurement bias of chemical analysis was noticed on the flush salt as well. The flush salt, with a nominal composition of ^{7}LiF-BeF_2 (66-34 mole%) was employed to flush the fuel system initially and later, on occasions before and after maintenance periods. The average composition of the flush salt as determined by chemical analysis was ^{7}LiF-BeF_2 (63.56 $\pm$ 0.005 / 36.44 $\pm$ 0.005 mole%). Examinations of the material balance indicated that this discrepancy was due to an analytical bias.

The reason for choosing the nominal salt composition, instead of the anticipated mole fraction specified in [3], in the benchmark is to keep the best consistency among reference on the key parameter for the critical experiment, which is the mass fraction of ^{235}U in this case. The ^{235}U mass fraction calculated from the nominal composition, which is 1.409 %, agrees the best with the tolerance range of (1.408 ± 0.007) % provided in [3].

4.1.4 Sensitivity coefficients for k_{eff} from cross section data uncertainties

Table 4.7 provides the sensitivity coefficients for the k_{eff} from nuclear data uncertainties in each important element in all the materials using Serpent 2 sensitivity coefficient calculation capabilities[18]. Combined with SCALE6.2 56-group covariance matrices through the so-called sandwich rule, uncertainty for k_{eff} from cross sections was estimated to be 664 pcm and the most important uncertainty contributors are listed in Table 4.8.

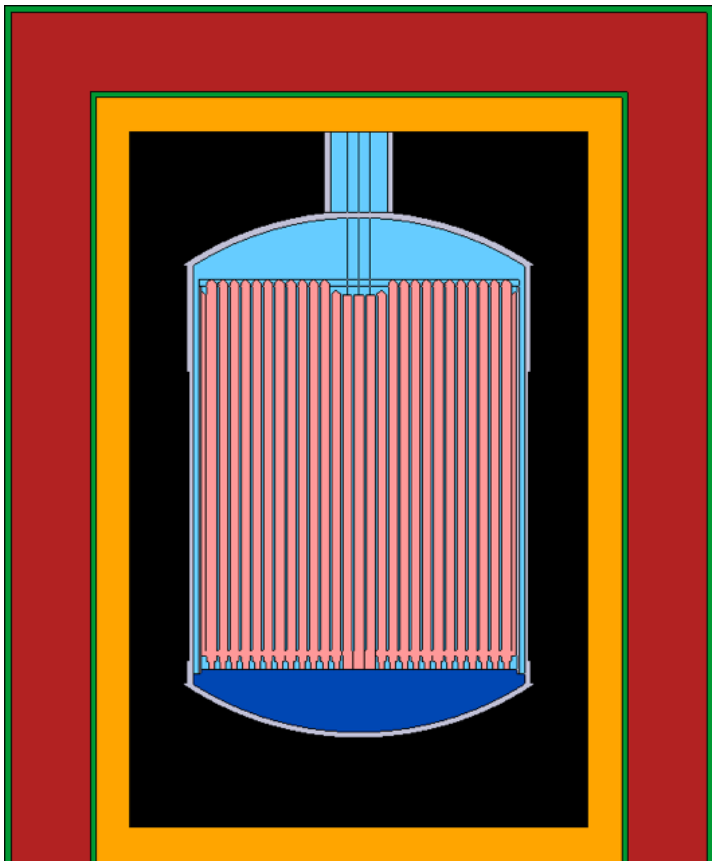

Figure 4.1: Vertical cross section of the MSRE model without the distributor (at $y = 0$).

4.1.5 k_{eff} of models with geometry simplifications

Given the complexity of the MSRE model, it might be challenging for many codes to reproduce the full details of the model. Here, the impacts of some geometry modifications were evaluated such that reference k_{eff} for the MSRE model with various levels of simplifications is provided.

1. Impact of removing the flow distributor

   The shape of the flow distributor, arranged at the top of the vessel to connect with the fuel salt inlet, is the half of a torus (see Figure 2.3), which may be difficult for some codes to build the geometry. If the distributor is removed from the model, $k_{eff} = 1.020\,320 \pm 0.000\,035$ (a $-0.098\,\%$ change as compared to the reference value since we lose some salt in the system).

2. Impact of changing the shape of the top and bottom head of the vessel

   The shapes of the top and bottom head of the reactor vessel are two identical torispherical domes. If they are modeled as flat rather than concave surfaces whereas the height of the vessel is conserved (see Figure 4.2), k_{eff}=1.023 800 $\pm$ 0.000 035 (a 0.243 $\%$ change as compared to the reference value since we add more salt in the system).

3. Impact of the sample basket

   The sample baskets are located in the most important region of the core and their geometry is complicated in the MSRE benchmark model. The following simplifications are considered:

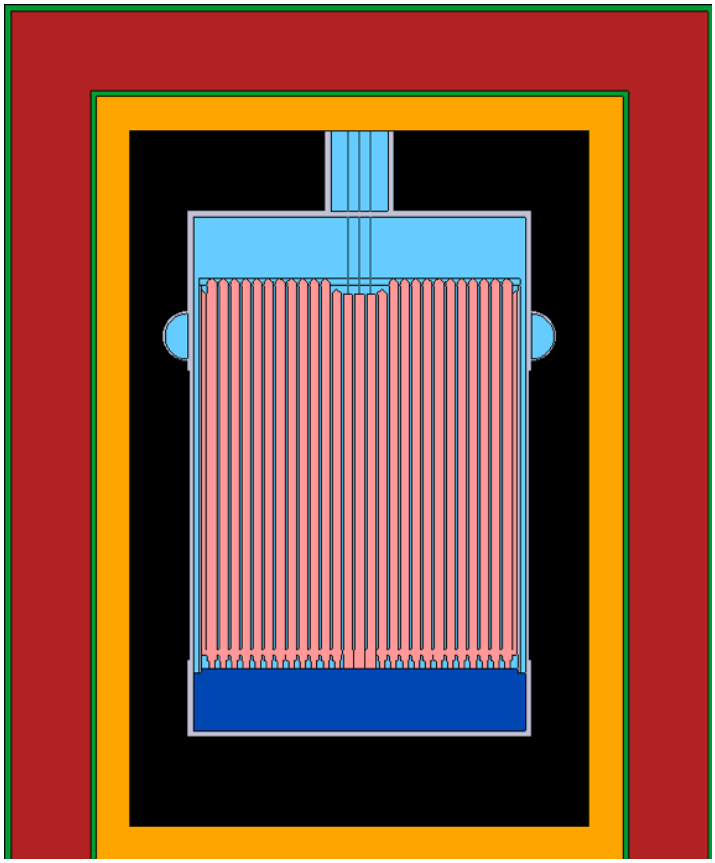

Figure 4.2: Vertical cross section of the MSRE model with flat top and bottom section (at $y = 0$).

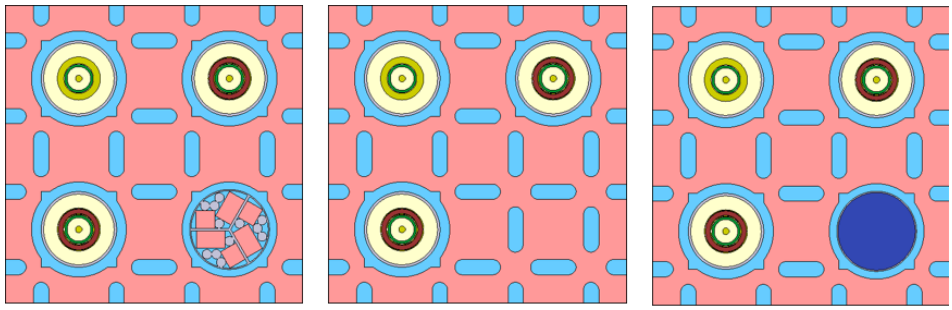

(a) Reference (b) Graphite channel (c) Homogenized

Figure 4.3: Comparison of models for the sample basket.

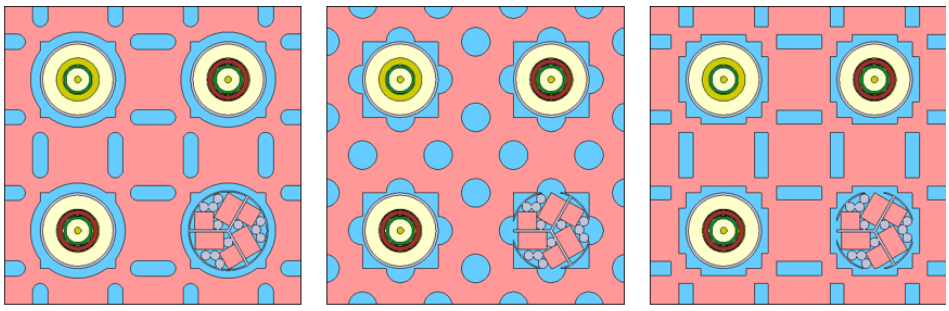

(a) Reference (b) Circular channel (c) Rectangular channel

Figure 4.4: Comparison of models for the fuel channel.

- the sample basket is modeled as a regular channel, therefore, made of graphite (Figure 4.3b): k_{eff}=1.037 900 $\pm$ 0.000 035 (a 1.623 % change as compared to the reference value);
- the materials in the sample basket are homogenized and the basket outer radius and the channel shape are kept unchanged (Figure 4.3c): k_{eff}=1.020 940 $\pm$ 0.000 034 (a $-$0.037 % change as compared to the reference value). The change of k_{eff} is very small.

4. Impact of the shape of the fuel channel

   The shape of the fuel channel is a rectangular with round corners which may be difficult to model for some codes. The following options are considered for simplifying the geometry of the fuel channel:

   - circular channel with 0.957 cm radius in order to maintain the same cross-sectional area of the reference channels (Figure 4.4b): k_{eff}=1.024 500 $\pm$ 0.000 034 (a 0.311 % change as compared to the reference value);
   - rectangular channel (Figure 4.4c) with the long side equal to the length of the long side of the reference channel (3.048 cm) and the half length of the short side (0.472 cm) adjusted to preserve the channel cross sectional area: k_{eff}=1.021 510 $\pm$ 0.000 035 (a 0.019 % change as compared to the reference value). The change of k_{eff} is very small.

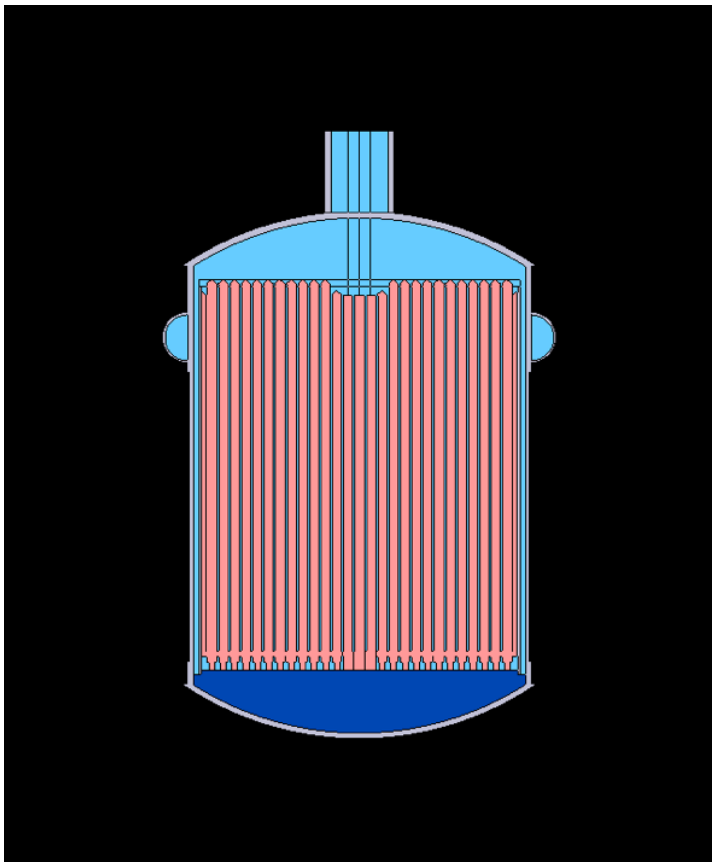

Figure 4.5: Vertical cross section of the MSRE model without thermal shield and insulation layer (at $y = 0$).

5. Impact of removing the thermal shield

   If the thermal shield and insulation layer are removed from the model (see Figure 4.5), k_{eff}=1.012 280 $\pm$ 0.000 033 (a $-0.885\,\%$ change as compared to the reference value due to loss of neutrons that could be reflected back to the core from the thermal shield).

Table 4.9 summarizes the calculations results of models with different geometry simplifications.

4.2 Reactivity Effect

4.2.1 Experimental uncertainty analysis

The evaluation of the MSRE reactivity effect benchmark starts with the uncertainty analysis of experimental values. An uncertainty of 2% was attributed to the reported reactivity measurements from ORNL. It was believed that the experimental measurement uncertainty was significantly larger than the computation process uncertainty and the uncertainty of reactor period measurement contributed the most to the experimental uncertainty.

Also, there's an uncertainty caused by the correction factors which were applied to the rod sensitivity measurements to pull the measurements all on the basis of one ^{235}U concentration. This correction factor was calculated by ORNL and now checked on the MSRE benchmark model. The reactivity change of rod No. 1 between fully withdrawn and fully inserted positions was evaluated

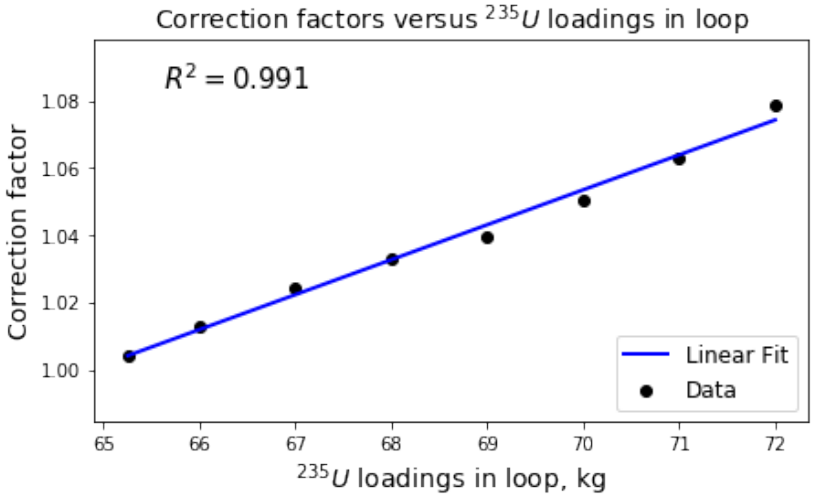

Figure 4.6: Correction factors with different ^{235}U loadings in loop.

with various ^{235}U loadings in loop and the correction factor for a certain ^{235}U concentration was defined as follows:

$$cf(x) = \frac{\rho_1(x_0) - \rho_0(x_0)}{\rho_1(x) - \rho_0(x)} \tag{4.2}$$

where x is the current ^{235}U loadings in loop, x_0 is initial critical ^{235}U loading that is 65.25 kg, $\rho_1(x)$ is the reactivity with rod No. 1 fully withdrawn and $\rho_0(x)$ is the reactivity with rod No. 1 fully inserted into the core.

It was found that the correction factor calculated in the benchmark model was almost linearly with the ^{235}U concentration as shown in Figure 4.6. The largest deviation from the correction factors calculated by the MSRE benchmark model to those provided by ORNL, applied for a certain ^{235}U level, was found to be less than 2 %. So, the uncertainty due to the applied correction factor was assumed to be 2 % by a conservative estimation. No significant bias or systematic error was observed for the correction factor applied on the measurements. The uncertainty of rod worth measurements is now the square root of the sum of the squares of the experimental uncertainty and the uncertainty in the correction factor, which is 2.83 %. It was found that the reactivity effect such as the control rod worth is not sensitive to the most important uncertainty contributors of the multiplication factor. The change of the control rod worth for rod No. 1 due to 1σ change of the graphite density is only 0.014 % of the original value and is negligible due to 1σ change of ^{6}Li enrichment. Therefore, it is reasonable to infer that the uncertainty of reactivity effects caused by uncertainty of model parameters are insignificant compared to 2.83 %.

The basic assumption supporting the application of correction factor is that the shape of integral worth vs position curve for control rods is unaffected by ^{235}U concentration. This assumption was checked on the MSRE benchmark model. The plot of normalized rod worth $f(z)$ vs. normalized rod position z with three different ^{235}U concentrations is shown in Figure 4.7, where z measures the height of rods above the lower limit and this curve was normalized to zero at lower limit ($z = 0$) and to unity at the upper limit ($z = 1$). The three curves in Figure 4.7 differ very little, demonstrating the feasibility of this assumption.

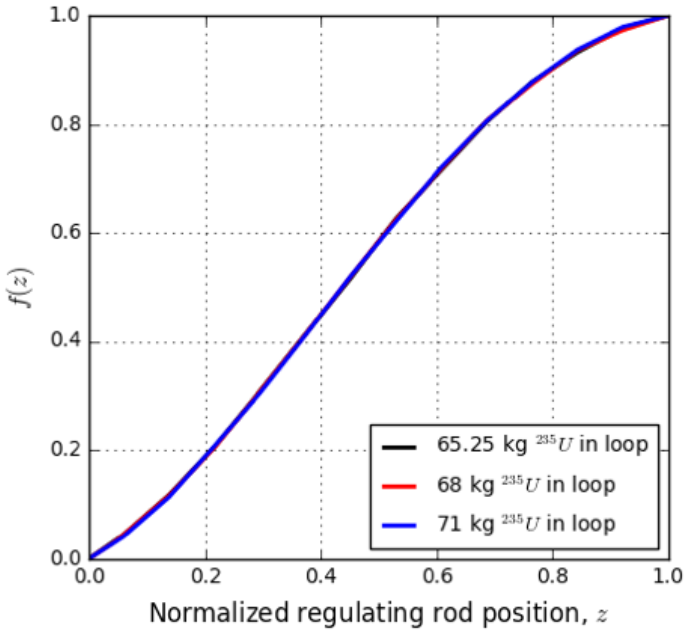

Figure 4.7: Regulating curve of rod No. 1 in the presence of (a) 65.25 kg ^{235}U in loop, (b) 68 kg ^{235}U in loop and (c) 71 kg ^{235}U in loop.

4.2.2 Integral and differential rod worth

For the differential control rod worth evaluation, rod No. 1 was moved from the fully withdrawn position to the bottom of the control rod thimble while other two rods were held fully withdrawn. The integral worth curve of rod No. 1 is shown in Figure 4.8. The differential worth of rod No. 1 is shown in Figure 4.9 and Figure 4.10 with different Δx in calculating the change of reactivity. The use of a smaller Δx does not improve the accuracy of differential rod worth calculation since the control rod does not consist of homogeneous material but features a special design as shown in Figure 2.9. The code-to-experiment comparison of the differential rod worth is shown in Table 4.10.

The calculated differential rod worth tends to be shifted to the left from the benchmark value overall and this shift led to the mismatch in the integral worth curve as well. The higher calculated differential worth at 0 in in Figure 4.9 indicates that the rod in the model was not inserted low enough at its fully inserted position. The initial fully withdrawn position of the control rods was obtained indirectly since, as stated before, the benchmark model was thermally expanded downward by assumption. If we artificially lower the upper limit of all rods by 10 cm, which means inserting all rods 10 cm more at the beginning, the mismatch in both the integral and differential worth could be corrected in the right direction as shown in Figure 4.11 and Figure 4.12. This phenomenon indicates the need to further investigate the initial position of all rods at room temperature and the thermal expansion mechanism of them.

4.2.3 Reactivity Equivalent of ^{235}U

Reactivity for cases with ^{235}U loadings of 65.25 kg, 66 kg, 67 kg, 68 kg, 69 kg, 70 kg, 71 kg and 72 kg in the loop was calculated, while the core configuration is set as all control rods withdrawn to their upper limit. The results are plotted in Figure 4.13.

The average value of reactivity equivalent of ^{235}U additions are obtained as the linear regression

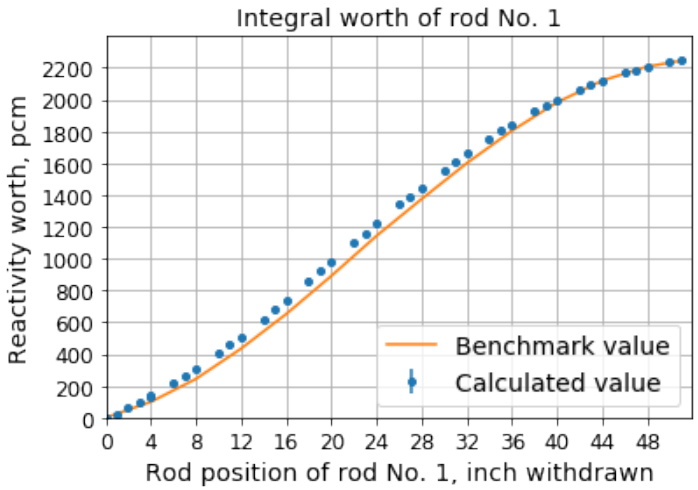

Figure 4.8: Integral worth of control rod No. 1.

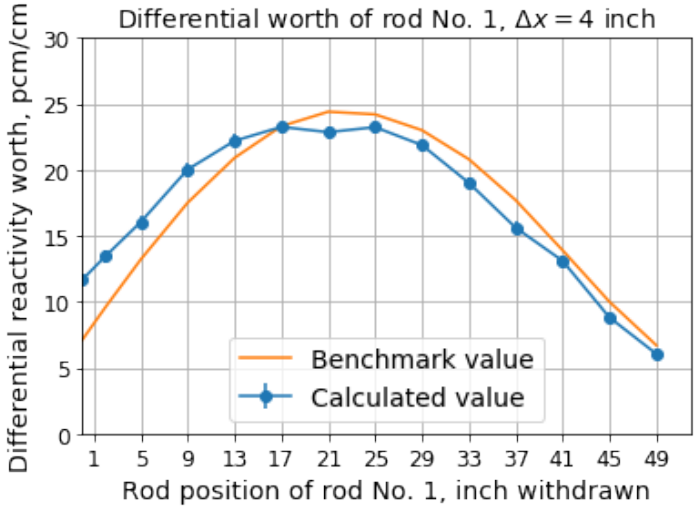

Figure 4.9: Differential worth of control rod No. 1, $\Delta x = 4$ inch.

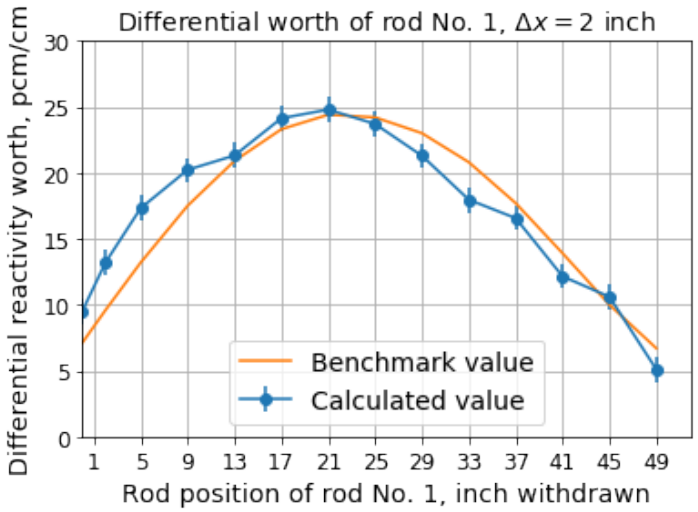

Figure 4.10: Differential worth of control rod No. 1, $\Delta x = 2$ inch.

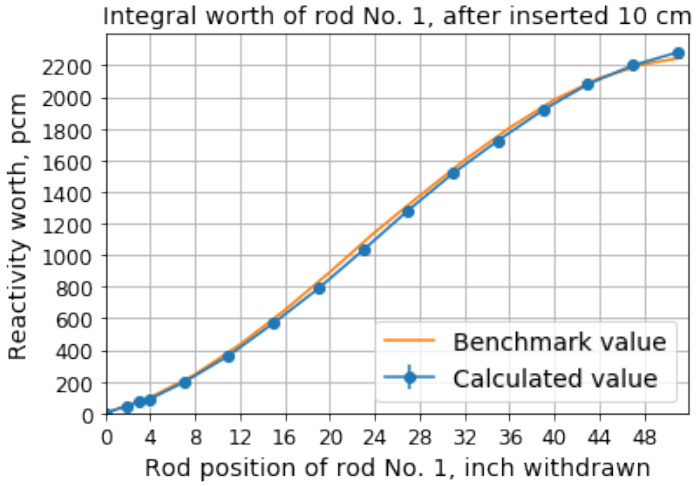

Figure 4.11: Integral worth of rod No. 1 after inserting all control rods 10 cm at the beginning positions.

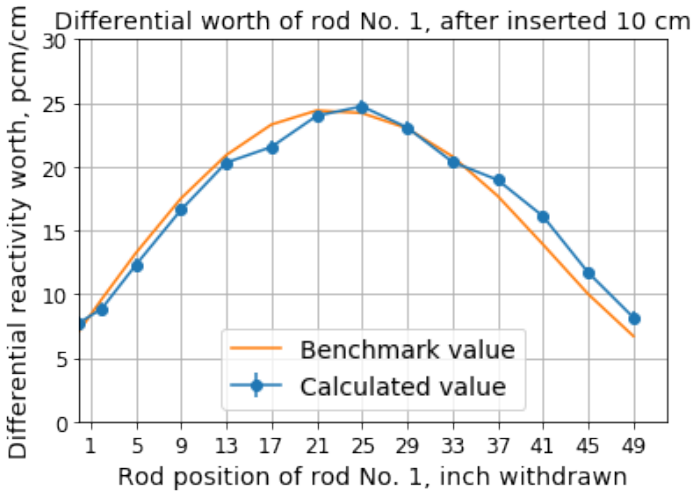

Figure 4.12: Differential worth of rod No. 1 after inserting all control rods 10 cm at the beginning positions.

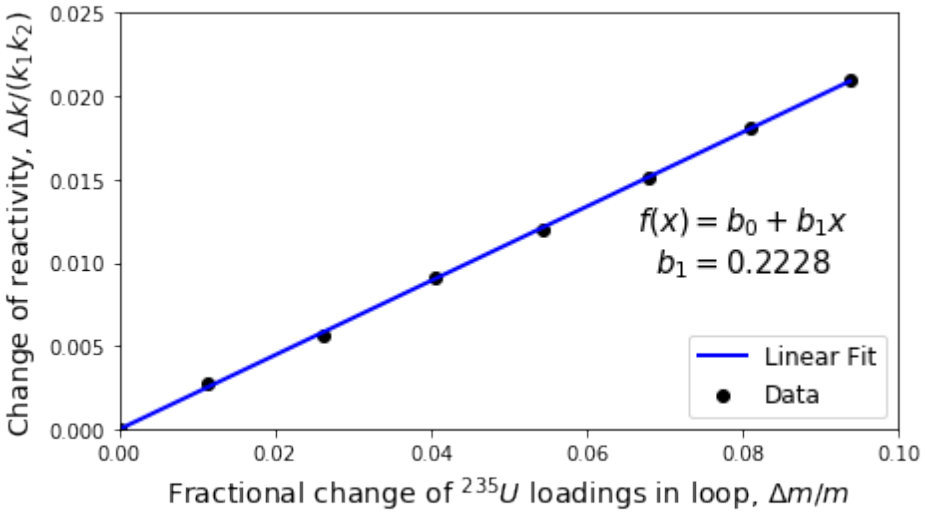

Figure 4.13: Effect of ^{235}U mass on reactivity.

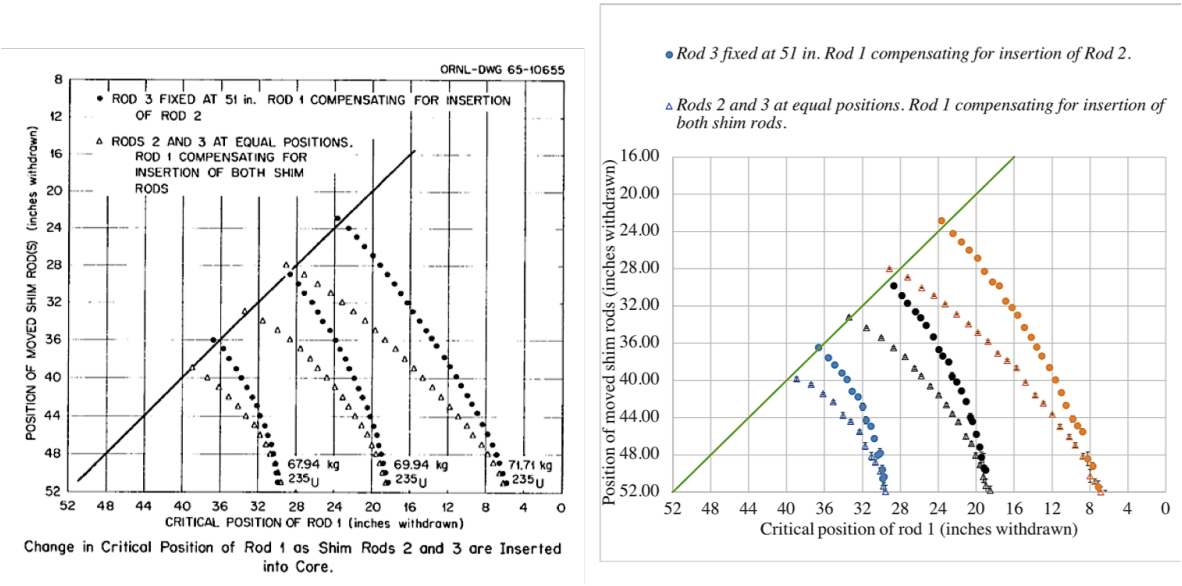

Figure 4.14: Rod-shadowing effect comparisons between calculated values and experimental values.

coefficient as shown in Figure 3.11. The calculated value of the reactivity equivalent of ^{235}U additions is provided in Table 4.11. The calculated value and the benchmark value are in good agreement (within 1σ).

4.2.4 Rod-shadowing effect

Rod-shadowing effect refers to the change in the critical position of the regulating rod (rod No. 1) as the shim rods (rods No. 2 and No. 3) were inserted into the core. Using the method described in Chapter 3, a preliminary code-to-experiment comparison of the rod-shadowing effect was conducted as shown in Figure 4.14. The calculated values and experimental values roughly agreed.

4.2.5 Worth of rod bank

Utilizing the results of the rod-shadowing effect experiment, the reactivity worthies of various shim and regulating rod combinations, also called rod bank, can be obtained assuming that the shape of the bank worth curve is sufficiently close to that for the single regulating rod [3]. The integral worth vs position curve for different rod banks was checked on the MSRE benchmark model. They come in slightly different shapes, as shown in Figure 4.15, but in general are very similar.

In the benchmark model, the control rod bank worth from rod bank No. 1 & 2 and rod bank for all three rods were calculated from the change of reactivity with rod bank fully withdrawn (51 in withdrawn) and fully inserted (0 in withdrawn) at three certain ^{235}U loading level. All the rods included in one bank were at held at identical elevations. The calculated k_{eff} for each case is shown in Table 4.12.

The calculated values of the control rod bank worth are provided in Table 4.13. The calculated values and the benchmark values are in good agreement (within 1σ for 5 case and within 2σ for only 1 case).

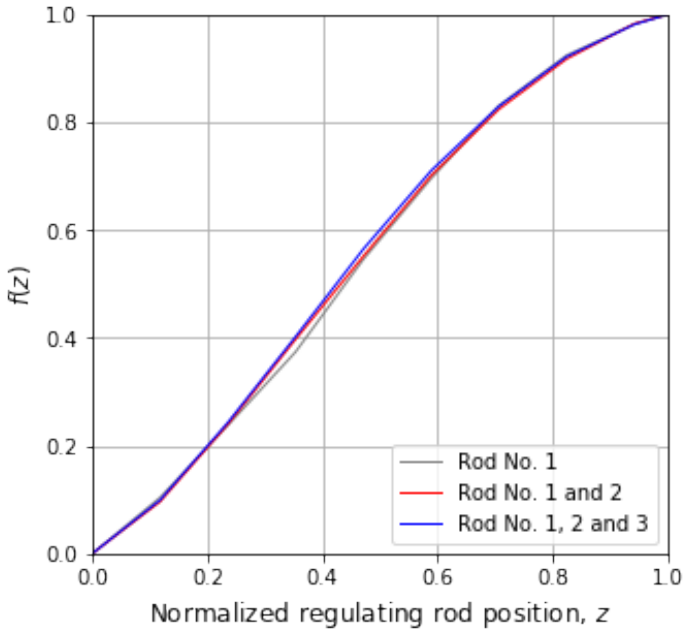

Figure 4.15: Regulating curve of (a) rod No. 1, (b) rod No. 1 and 2 and (c) rod No. 1, 2 and 3.

4.2.6 Reactivity effects of fuel circulation

Using the method described in Chapter 2, the calculated value for the reactivity loss due to fuel circulation is provided in Table 4.14. The calculated value shows good agreement with the benchmark value (within 1σ).

It was assumed that the fuel salt speed is 6.11 cm/s in the lower head, 17.71 cm/s in the channeled region and 6.12 cm/s in the upper head. The time spent outside of the core is 32 % of the total time required to complete a loop (25.2 s in total as shown in Table 2.1). The change of β_{eff} due to fuel circulation was calculated to be -224.83 pcm.

Figure 4.16 compares the probability of DNP decay in the centerline of the reactor for different precursor groups in the circulating and in the stationary case. It can be noticed that the fuel circulation has little to no effect on the DNP distribution for short lived DNPs compared to the case when the fuel is stationary, whereas it effectively flattens the distribution for long lived ones.

4.2.7 Rod-drop effects

Rod-drop experiments consisted of the simultaneous scram of the regulating rod group from its initial critical position. The integrated count as a function of time following the drop was recorded in the experiment.

Using the method described in Chapter 3, a code-to-experiment comparison of the rod-drop effect was conducted as shown in Figure 4.17 and Figure 4.18. As described above, the magnitude of the negative reactivity insertion of different rod groups ranging from the initial critical position to the scram position (-4 in) and β_{eff} were determined by the Serpent 2 model. The critical positions of the rod group with various ^{235}U concentration was obtained by method of linear regression using the position vs reactivity curve.

Accuracy of this calculation is sensitive to the magnitude of the reactivity insertion at the scram position, which depends on the fuel salt composition during the experiment which was not provided directly. The fuel salt composition was obtained by adding a certain amount of fuel

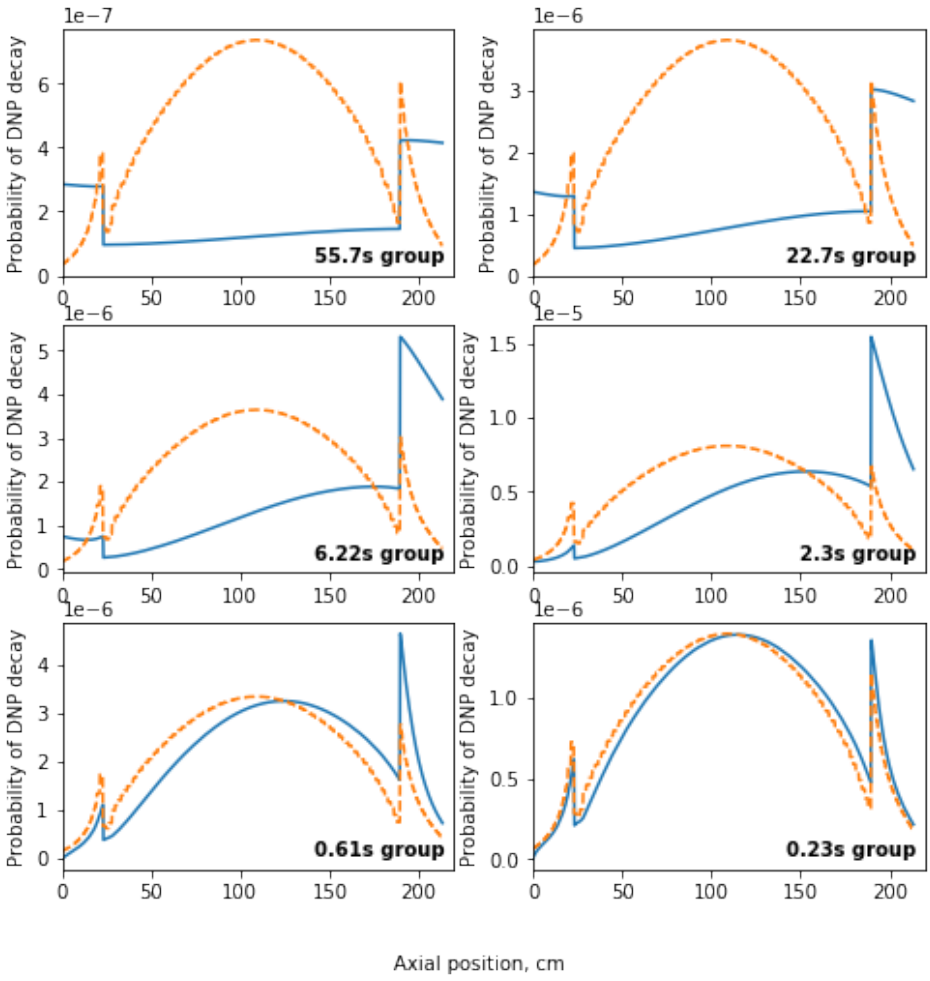

Figure 4.16: The probability of DNP decay in the centerline of the reactor in the stationary (dashed line) and the circulating (solid line) case for six decay groups—the spikes are due to the larger volume of salt in the bottom and top plena.

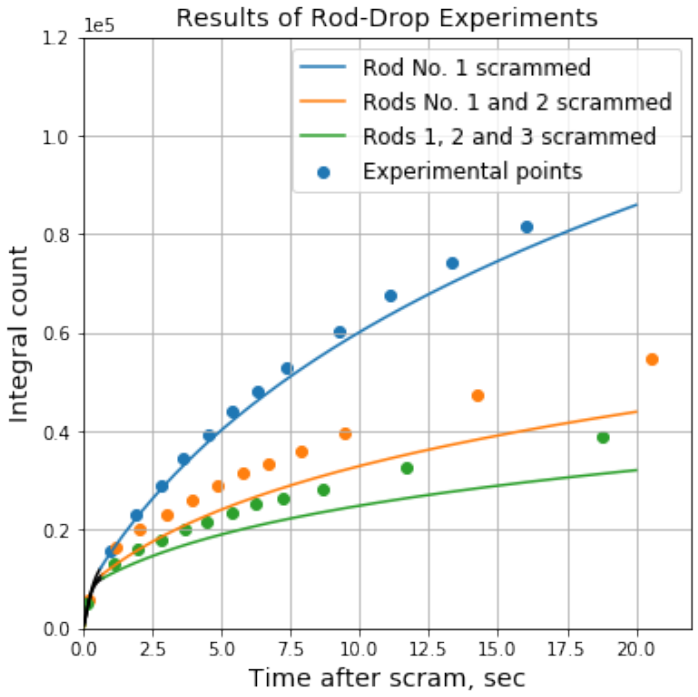

Figure 4.17: Results of rod-drop experiments after 30 capsule additions.

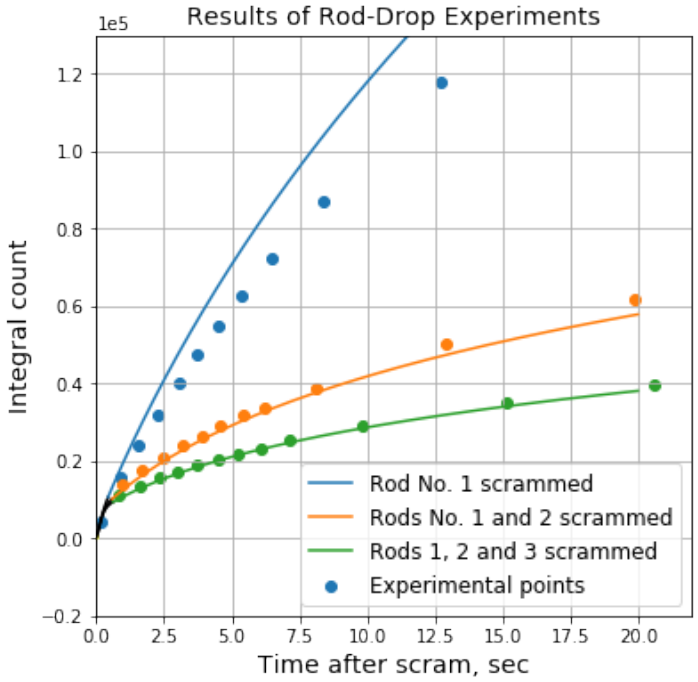

Figure 4.18: Results of rod-drop experiments after 65 capsule additions.

capsules to the initial critical composition therefore the amount of ^{235}U contained in each capsule needs to be carefully checked. Also, the result is sensitive to the effective lag time between scram signal and start of the rod drop, the initial count rate and the acceleration of rod-drop.

The discrepancy of the calculated result and the experimental data yields no uniform behaviour in different cases. The discrepancy may originate from calculating the initial critical position of the regulating rod group with various ^{235}U loadings, but such important information was provided in the MSRE reports. From previous calculations of rod bank worth (see Table 4.13) and the integral worth curve of rod No. 1 (see Figure 4.8), the MSRE benchmark model was proved to be able to yield an accurate estimation of the control rod worth for a single rod or a rod group. In addition, the composition of the fuel salt with ^{235}U loading specified was proved to be practical according to the code-to-experiment validation of reactivity coefficient of ^{235}U (see Table 4.11). Therefore, there may be a problem or inconsistency between the expected and as-built/actual amount of ^{235}U contained in each fuel capsule, which led to the inaccuracy of fuel salt composition representation in the rod-drop benchmark model.

4.2.8 Temperature reactivity effects

The benchmark model temperature is 922 K and it was varied $\pm$50 K at three various ^{235}U loadings in the loop. The change in the reactor core geometry was considered with the change of temperature according the thermal expansion coefficients of materials. Both the temperature and density changes were considered for all materials inside the reactor vessel. All control rods were fully withdrawn. The calculated values for isothermal temperature coefficients at three ^{235}U loadings are provided in Table 4.15. The calculated values are slightly smaller than the benchmark value but they agree within 1σ. There's no obvious relationship between the ^{235}U loading in the fuel salt and the isothermal temperature coefficient.

To calculated the fuel salt temperature coefficient, only the fuel salt temperature was varied $\pm$50 K in the system. The density of the fuel salt was adjusted with the change of temperature. All three control rods were fully withdrawn. The ^{235}U loading was arbitrarily chosen as the initial critical amount. The calculated value of the fuel temperature coefficient is provided in Table 4.16. The calculated value is slightly smaller than the benchmark value, similar to the bias of isothermal temperature coefficient calculation, but they agree within 1σ.

4.3 Conclusions

A set of MSRE benchmarks was created basing on the first zero-power criticality experiment and the series of control rod calibration experiments performed at the MSRE in 1965. The fully-detailed benchmark model for the MSRE, using Monte Carlo code Serpent 2, was utilized to analyze the effective multiplication factor when ^{235}U was progressively added to the fuel salt in order to achieve criticality with stationary salt and isothermal conditions. The calculated multiplication factor in such conditions was 1.021 32 ($\pm$3 pcm). The total uncertainty for experimental k_{eff} was estimated to be 420 pcm.

Basing on the Serpent 2 model of the MSRE, new methods were developed to analyze the reactivity effects and reactivity coefficients measurement. An uncertainty of 2 % was attributed to the reported reactivity measurements from experimenters and it was believed that the uncertainty of reactor period measurement contributed the most of the experimental uncertainty. An addition 2 % uncertainty was added to all reactivity measurements to represent the uncertainty for the correction factor applied to pull all the measurements on the same uranium concentration and this uncertainty was reasonably inferred by evaluating this factor on the MSRE benchmark model. The calculated reactivity equivalent of ^{235}U additions (0.2228 ± 0.0014, represented as the change of reactivity over the relative change of ^{235}U mass in loop) matches well with the experiment

value (0.223 ± 0.006), strengthening the confidence of accurate representation of the fuel salt composition in the MSRE model. Most of other calculations, including the control rod bank worth, reactivity effects of fuel circulation and isothermal and fuel temperature coefficients show good agreement with experiment values (within 1σ) as well.

Table 4.4: Individual and total uncertainties of k_{eff}.

Item	Nominal and bounding values	Δk_i, pcm
Graphite density	1.86, 1.83-1.87 g/cm^3	334
Fuel salt density	(2.3275 ± 0.0160) g/cm^3	103
Be mass in carrier salt	(309.62 ± 5.00) kg	8
Zr mass in carrier salt	(541.36 ± 5.00) kg	12
^{235}U mass fraction in the salt	(1.409 ± 0.007) wt %	81
^{234}U mass fraction in the salt	(0.014 ± 0.007) wt %	74
^{236}U mass fraction in the salt	(0.006 ± 0.006) wt %	17
INOR-8 density	(8.7745 ± 0.0200) g/cm^3	3
Graphite core height	(166.724 ± 1.000) cm	21
Graphite core radius	(70.285 ± 0.200) cm	4
Fuel channel width	(1.0160 ± 0.0127) cm	51
Fuel channel length	(3.0480 ± 0.0127) cm	23
^{6}Li enrichment	(0.005 ± 0.001) at %	172
Boron concentration in graphite	$(0.000\,080 \pm 0.000\,008)$ wt %	17
Temperature of thermal shield	305 K, 600 K	2
Temperature of fuel salt	(911 ± 1) K	6
Temperature of graphite	(911 ± 1) K	1
Height vertical section of bottom head	(6.475 ± 1.000) cm	9
Outlet pipe thickness	(2.511 ± 0.250) cm	3
Outlet pipe height	(36.180 ± 1.000) cm	4
Distributor thickness	(0.826 ± 0.080) cm	3
Sample basket outer diameter	(5.4287 ± 0.0127) cm	0.0
Sample basket gap	0, 0.0127 cm	5
Cell atmosphere gas composition	Mass fraction vs. atom fraction	0.0
INOR-8 composition (C mass fraction)	0.06 %, 0.08 %	5
Mo mass fraction in INOR-8	(17.0 ± 0.5) wt %	12
Cr mass fraction in INOR-8	(7.0 ± 0.5) wt %	5
Fe mass fraction in INOR-8	(5.0 ± 0.5) wt %	4
Impurities in salt	Fe: (162 ± 65) ppm, Cr: (28 ± 7) ppm Ni: (30 ± 20) ppm, O: (490 ± 49) ppm	12
Helium void in salt	0, 0.076 vol %	5
Salt absorption in graphite	0, 0.0010 vol %	2
Hf in Zr	50 ppm, 0 ppm	12
Impurities in graphite	Ash: $(0.000\,50 \pm 0.000\,05)$ wt % V: $(0.000\,90 \pm 0.000\,09)$ wt % S: $(0.000\,50 \pm 0.000\,05)$ wt %	4
Graphite stringer width	$(5.07492^{+0.0000}_{-0.0127})$ cm	13
Poison density	(5.873 ± 0.020) g/cm^3	0.5
Gd_2O_3 mass fraction	(70 ± 1) wt %	0.6
Control rod position	(118.364 ± 0.127) cm	0.7
Regulating rod	Rod 1, Rod 2 or Rod 3	0.0
Graphite thermal expansion coefficient	$(1.5 \pm 0.2) \times 10^{-6}$ °F^{-1}	18
INOR-8 thermal expansion coefficient	$(7.8 \pm 0.2) \times 10^{-6}$ °F^{-1}	17
Measurement uncertainty in k_{eff}	-	10
Total (root mean square)	-	420

Table 4.5: Impact of temperature of thermal scattering cross section.

C-nat in graphite	C-nat in thermal shield	H-1 in thermal shield	k_{eff} (1σ)	Difference, pcm
800 K	296 K	293.6 K	1.027 23(10)	0
911 K	305 K	305 K	1.021 32(3)	−591
1000 K	400 K	350 K	1.016 40(10)	−1083

Table 4.6: Impact of fuel salt composition, the impurities are assumed to be 0.071 wt $\%$ for all salt options

Salt option	Li, wt.%	Be, wt.%	Zr, wt.%	U, wt.%	k_{eff} (1σ)	Diff., pcm
Benchmark salt (nominal)	10.957	6.349	11.101	4.495	1.02132(3)	0
Chemical analytical composition	10.327	6.695	11.016	4.440	1.02248(10)	116
Anticipated mole fraction[a]	10.970	6.324	10.972	4.641	1.02595(10)	463

[a] Composition is 65.0LiF-29.17BeF_2-5.0ZrF_4-0.83UF_4

Table 4.7: Sensitivity coefficients for k_{eff} from cross section data uncertainties, $\frac{dk/k}{d\sigma/\sigma}$.

Nuclide	Total $(\times 10^{-5})$	Elastic scattering $(\times 10^{-5})$	Neutron capture[a] $(\times 10^{-5})$	Fission $(\times 10^{-5})$
Li-6	−1430	0.04	−1430	n/a
Li-7	770	2010	−1380	n/a
Be-9	2920	3250	−340	n/a
Zr-90	3	50	−64	n/a
Zr-91	−520	150	−670	n/a
Zr-92	−16	130	−160	n/a
Zr-94	−36	5	−54	n/a
Zr-96	−86	2	−89	n/a
F-19	8410	8080	−1070	n/a
C-nat	51 400	39 210	−1760	n/a
B-10	−650	0.2	−650	n/a
U-235	22 990	47	−14 080	37 020
U-238	−8470	610	−9170	63

[a] Reactions with no neutron yield.

Table 4.8: Uncertainties for k_{eff} from cross section data uncertainties

Reaction	Uncertainties, pcm
^{235}U $\bar{\nu}$ × ^{235}U $\bar{\nu}$	373
C elastic × C elastic	264
^{235}U χ × ^{235}U χ	257
^{7}Li(n, γ) × ^{7}Li(n, γ)	197
^{235}U(n, γ) × ^{235}U(n, γ)	172
^{19}F elastic × ^{19}F elastic	150
^{235}U(n, f) × ^{235}U(n, γ)	128
^{235}U(n, f) × ^{235}U(n, f)	120
^{58}Ni(n, γ) × ^{58}Ni(n, γ)	97
^{19}F inelastic × ^{19}F inelastic	96

Table 4.9: Impact of geometry changes on k_{eff}.

Case	k_{eff}	$100(k_{eff} - k_{ref})/k_{ref}$ [a]
No distributor	1.02032±0.000035	−0.098
With flat top and bottom surfaces of the vessel	1.02380±0.000035	0.243
Replace the sample basket by graphite channel	1.03790±0.000035	1.623
Make the sample basket homogeneous	1.02094±0.000034	−0.037
Circular fuel channels	1.02450±0.000034	0.311
Rectangular fuel channel	1.02151±0.000036	0.019
No thermal shield and insulation layer	1.01228±0.000033	−0.885

[a] k_{ref}= 1.021 320 ± 0.000 034.

Table 4.10: Differential worth of control rod No. 1 for the MSRE at initial critical ^{235}U loading.

Rod position, inch	Calculated value, pcm/cm	Benchmark value, pcm/cm	C/E
49	6.05 ± 0.46	6.7 ± 0.2	0 90 ± 0 07
45	8.81 ± 0.46	10.0 ± 0.3	0 88 ± 0 05
41	13.10 ± 0.46	13.9 ± 0.4	0 94 ± 0 04
37	15.61 ± 0.46	17.7 ± 0.5	0 88 ± 0 04
33	19.01 ± 0.45	20.8 ± 0.6	0 92 ± 0 03
29	21.87 ± 0.46	23.0 ± 0.6	0 95 ± 0 03
25	23.23 ± 0.47	24.2 ± 0.7	0 96 ± 0 03
21	22.85 ± 0.47	24.4 ± 0.7	0 94 ± 0 03
17	23.25 ± 0.47	23.3 ± 0.7	1 00 ± 0 03
13	22.19 ± 0.48	20.9 ± 0.6	1 06 ± 0 04
9	20.02 ± 0.48	17.5 ± 0.5	1 15 ± 0 04
5	16.04 ± 0.47	13.2 ± 0.4	1 22 ± 0 05
2	13.46 ± 0.47	9.6 ± 0.3	1 41 ± 0 06
0	11.66 ± 0.48	7.1 ± 0.2	1 64 ± 0 08

Table 4.11: Reactivity equivalent of ^{235}U additions, $\delta\rho/(\delta m/m)$.

Calculated value	Benchmark value	C/E
0.2228 ± 0.0014	0.223 ± 0.006	0.999 ± 0.029

Table 4.12: k_{eff} for control rod bank worth calculations.

Rod group	^{235}U in loop, kg	Rod group position	Calculated k_{eff}
1-2	67.94	Fully withdrawn	1.02997±0.000095
		Fully inserted	0.988803±0.00010
1-2	69.94	Fully withdrawn	1.03626±0.000093
		Fully inserted	0.995559±0.000097
1-2	71.71	Fully withdrawn	1.04186±0.000094
		Fully inserted	1.00148±0.000097
1-2-3	67.94	Fully withdrawn	1.02997±0.000095
		Fully inserted	0.973297±0.00010
1-2-3	69.94	Fully withdrawn	1.03626±0.000093
		Fully inserted	0.980123±0.000099
1-2-3	71.71	Fully withdrawn	1.04186±0.000094
		Fully inserted	0.985755±0.00010

Table 4.13: Control rod bank total worth at full insertion.

Rod group	^{235}U in loop, kg	Calculated value, pcm	Benchmark value, pcm	C/E
1-2	67.94	4042±14	4099±116	0.99±0.03
1-2	69.94	3945±13	3975±112	0.99±0.03
1-2	71.71	3870±13	4075±115	0.95±0.03
1-2-3	67.94	5653±14	5596±158	1.01±0.03
1-2-3	69.94	5526±14	5611±159	0.98±0.03
1-2-3	71.71	5463±14	5570±158	0.98±0.03

Table 4.14: Reactivity loss due to fuel circulation.

Calculated value, pcm	Benchmark value, pcm	C/E
222±10	212±6	1.05±0.06

Table 4.15: Isothermal temperature coefficient.

^{235}U in loop, kg	Calculated value, $^{\circ}F^{-1}$	Benchmark value, $^{\circ}F^{-1}$	C/E
67.86	-(6.95±0.13) $\times 10^{-5}$	-(7.45±0.85) $\times 10^{-5}$	0.93±0.11
69.85	-(6.69±0.13) $\times 10^{-5}$	-(7.24±0.83) $\times 10^{-5}$	0.92±0.11
71.71	-(6.56±0.13) $\times 10^{-5}$	-(7.30±0.83) $\times 10^{-5}$	0.90±0.10

Table 4.16: Fuel temperature coefficient.

Calculated value, $^{\circ}F^{-1}$	Benchmark value, $^{\circ}F^{-1}$	C/E
$-(4.30\pm0.14) \times 10^{-5}$	$-(4.7\pm0.7) \times 10^{-5}$	0.92 ± 0.14

Conclusions and Future Work

This project successfully developed the world-first, MSR-related reactor physics benchmark based on a series of zero-power experiments conducted at the MSRE. The benchmark is available in the IRPhEP handbook starting from the 2019 edition.

The three-dimensional high-fidelity benchmark model of the MSRE was developed using the Monte Carlo neutron transport code Serpent 2 and multiple nuclear data evaluations (ENDF/B.VII and JENDL). To accurately model reactivity effect experiments, methodologies were developed in conjuction with the Serpent model to account for the fuel salt motion in the core.

The calculated multiplication factor for the criticality experiment, when ^{235}U was progressively added to the fuel salt in order to achieve criticality with stationary salt and isothermal conditions, is 1.02132 ($\pm$3 pcm). The total uncertainty for experimental k_{eff} was estimated to be 420 pcm. The calculated k_{eff} is 2.154 % larger than the experimental and benchmark model value, which is approximately five times the benchmark model uncertainty. Such bias is not uncommon in benchmarks of systems containing large volume of graphite (or other carbonaceous materials). According to the IRPhEP handbook[5], the calculated k_{eff} is 1.190 % larger than the expected value for HTR10. For HTTR, the calculated k_{eff} is 2.03 % larger than the expected value. The bias is possibly due to uncertainties in the impurity content of the graphite blocks, uncertainties in the neutron capture cross section of carbon and uncertainty in the properties of nuclear-grade graphite.

Uncertainty quantification is the essential part of an IRPhEP benchmark, the uncertainty caused by each important parameter in the benchmark model was evaluated independently. In addition, sensitivity coefficients and total uncertainty on k_{eff} due to nuclear data uncertainties in each element, in all the materials were quantified.

According to MSRE documentation, an uncertainty of 2 % was attributed to the reported reactivity measurements from experimenters and it was believed that the uncertainty of reactor period measurement contributed the most of the experimental uncertainty. An additional 2 % uncertainty was added to all reactivity measurements to represent the uncertainty for the correction factor applied to pull all the measurements on the same uranium concentration and this uncertainty was reasonably inferred by evaluating this factor on the MSRE benchmark model. The calculated reactivity equivalent of ^{235}U additions (0.2228 ± 0.0014, represented as the change of reactivity over the relative change of ^{235}U mass in the loop) matches well with the experimental value (0.223 ± 0.006), strengthening the confidence of accurate representation of the fuel salt composition in the MSRE model. Most of the other calculations, including the control rod bank worth, reactivity effects of fuel circulation and isothermal and fuel temperature coefficients show good agreement with experimental values (within 1σ) as well.

Based on the time and resources available for this project, the benchmark was limited to first zero-power critical experiments and the following experimental campaign with ^{235}U-bearing molten salt fuel. Nevertheless, the baseline developed in this benchmark, such as the system model and the simulation tools, can serve as a foundation for future benchmarks based on other experimental campaigns carried at the MSRE, as for example, campaigns aimed to understand reactor dynamics of the MSRE, effects of xenon poisoning, or the behavior of the system with ^{233}U fuel.

Bibliography

[1] A technology roadmap for generation iv nuclear energy systems. Technical Report GIF-002-00, 2002.

[2] Paul N Haubenreich and JR Engel. Experience with the molten-salt reactor experiment. *Nuclear Applications and technology*, 8(2):118–136, 1970.

[3] B.E. Prince, S.J. Ball, J.R. Engel, P.N. Haubenreich, and T.W. Kerlin. Zero-power physics experiments on the molten-salt reactor experiment. Technical Report ORNL-4233, Oak Ridge National Lab., Tenn., 1968.

[4] J. R. Engel and B. E. Prince. Zero-power experiments with 233u in the msre. Technical Report ORNL-TM-3963, Oak Ridge National Lab., Tenn., 1972.

[5] J Blair Briggs, John D Bess, and Jim Gulliford. Integral benchmark data for nuclear data testing through the icsbep & irphep. *Nuclear Data Sheets*, 118:396–400, 2014.

[6] R.C. Robertson. Msre design and operations report. part i. description of reactor design. Technical Report ORNL-TM-728, Oak Ridge National Lab., Tenn., 1965.

[7] G.M. Tolson and A. Taboada. Msre control elements: manufacture, inspection, drawings, and specifications. Technical Report ORNL-4123, Oak Ridge National Lab., Tenn., 1967.

[8] Roy E. Thoma. Chemical aspects of msre operations. Technical Report ORNL-4658, Oak Ridge National Lab., Tenn., 1971.

[9] B.E Prince, J.R Engel, and C.H Gabbard. Reactivity balance calculations and long-term reactivity behavior with 235u in the msre. Technical Report ORNL-4674, Oak Ridge National Lab., Tenn., 1972.

[10] P.N. Haubenreich, J.R. Engel, B.E. Prince, and H.C. Claiborne. Msre design and operations report: Part iii. nuclear analysis. Technical Report ORNL-TM-730, Oak Ridge National Lab., Tenn., 1964.

[11] H.E. McCoy and B. McNabb. Postirradiation examination of materials from the msre. Technical report, Oak Ridge National Lab., Tenn., 1972.

[12] Re B Briggs. Molten-salt reactor program, semiannual progress report for period ending august 31, 1965. *ORNL*, 3872:127, 1965.

[13] R.B. Briggs. Molten-salt reactor program semiannual progress report. Technical Report ORNL-3626, Oak Ridge National Lab., Tenn., 1964.

[14] Dan Shen, Massimiliano Fratoni, Manuele Aufiero, Adrien Bidaud, Jeffrey Powers, and Germina Ilas. Zero-power criticality benchmark evaluation of the molten salt reactor experiment. In *Proceedings of the International Conference on Physics of Reactors. PHYSOR 2018, Cancun, Mexico, April 2018*, 2018.

[15] Manuele Aufiero, Mariya Brovchenko, Antonio Cammi, Ivor Clifford, Olivier Geoffroy, Daniel Heuer, Axel Laureau, Mario Losa, Lelio Luzzi, Elsa Merle-Lucotte, et al. Calculating the effective delayed neutron fraction in the molten salt fast reactor: analytical, deterministic and monte carlo approaches. *Annals of Nuclear Energy*, 65:78–90, 2014.

[16] Jaakko Leppänen, Maria Pusa, Tuomas Viitanen, Ville Valtavirta, and Toni Kaltiaisenaho. The serpent monte carlo code: Status, development and applications in 2013. In *SNA+ MC 2013-Joint International Conference on Supercomputing in Nuclear Applications+ Monte Carlo*, page 06021. EDP Sciences, 2014.

[17] Minoru Goto, Satoshi Shimakawa, and Yasuyuki Nakao. Impact of revised thermal neutron capture cross section of carbon stored in jendl-4.0 on httr criticality calculation. *Journal of nuclear science and technology*, 48(7):965–969, 2011.

[18] Manuele Aufiero, Adrien Bidaud, Mathieu Hursin, Jaakko Leppänen, Giuseppe Palmiotti, Sandro Pelloni, and Pablo Rubiolo. A collision history-based approach to sensitivity/perturbation calculations in the continuous energy monte carlo code serpent. *Annals of Nuclear Energy*, 85:245–258, 2015.